TECTONICS, VOL. 32, 1384–1403, doi:10.1002/tect.20085, 2013

Synextensional magmatism leading to crustal flow in the Albion–Raft River–Grouse Creek metamorphic core complex, northeastern Basin and Range

Alexandros Konstantinou,[1] Ariel Strickland,[2] Elizabeth Miller,[1] Jeffrey Vervoort,[3] Christopher M. Fisher,[3] Joseph Wooden,[1,4] and John Valley[2]

Received 14 March 2013; revised 9 September 2013; accepted 12 September 2013; published 3 October 2013.

[1] This study addresses the origin of granitic magmas in the Albion–Raft River–Grouse Creek (ARG) metamorphic core complex and environs and how these inform us about the deep crustal processes leading to crustal flow and the formation of the ARG. SHRIMP-RG U-Pb zircon ages, whole-rock geochemical data (major and trace element data, as well as Sr and Nd isotopes), and zircon geochemistry (in situ O-isotope, Hf-isotope, and trace element compositions) from Eocene to Oligocene magmas now exposed at three structural levels of the ARG show that the 41–32 Ma Emigrant Pass and the 32–25 Ma Cassia plutonic complexes have a common origin, sharing a deep crustal "hot zone" that remained above solidus temperatures for at least 16 Myr. This magmatism is part of the protracted magmatism that swept southward across the western U.S. between ~42 and 21 Ma, inferred to be the result of foundering of the shallow Farallon slab. Isotopic modeling of geochemical data from these magmas suggests that between 41 and 32 Ma, the influx of mantle-derived basalt into the lower crust triggered large-scale hybrid magmatism generating calc-alkaline magmas that erupted and intruded the upper crust and significantly weakened the lower and middle crust. Between 32 and 25 Ma, this "hot zone" incorporated large amounts of continental crustal melts, resulting in greater mobility of the lower and middle crust, driving middle crustal flow and the formation of granitic plutons that rose to shallower levels of the crust forming the granite-cored gneiss domes of the ARG.

Citation: Konstantinou, A., A. Strickland, E. Miller, J. Vervoort, C. M. Fisher, J. Wooden, and J. Valley (2013), Synextensional magmatism leading to crustal flow in the Albion–Raft River–Grouse Creek metamorphic core complex, northeastern Basin and Range, *Tectonics*, *32*, 1384–1403, doi:10.1002/tect.20085.

1. Introduction

[2] Metamorphic core complexes are dome-shaped structural culminations of middle crustal metamorphic and igneous rocks that develop in extensional tectonic settings. They were first described in the Cenozoic Basin and Range province of the western U.S., where they occur in a sinuous zone ~150–200 km west of the easternmost limit of the Mesozoic thrust belt (Figure 1a). In general, metamorphic core complexes of the Cordillera expose Cenozoic plutonic rocks, are characterized by zones of high-strain ductile extension, al deformation and are bound by low-angle normal (detachment) faults [e.g., *Coney*, 1980; *Wernicke*, 1981; *Armstrong*, 1982; *Coney and Harms*, 1984]. The origin of core complexes, specifically the mechanisms involved in the rise of deep rocks to the surface during extension and the role of magmatism in their genesis, remains controversial.

[3] Recent studies throughout the globe have described metamorphic core complexes as gneiss or migmatite domes formed by extension-assisted diapiric ascent of partially molten crust [e.g., *Vanderhaeghe et al*., 1999; *Teyssier and Whitney*, 2002; *Whitney et al*., 2004; *Kruckenberg et al*., 2008; *Gordon et al*., 2008; *McFadden et al*., 2010; *Kruckenberg et al*., 2011]. Numerical modeling by *Rey et al*. [2009a, 2009b, 2011] illustrates how extensional gneiss domes can result from the collapse of overthickened crust, localized by a point-like or a fault-like anomaly in the brittle crust. In these models, the diapiric rise of deep crust is aided by decompression partial melting that weakens the crust. Anatectic melts crystallize as migmatites or coalesce to form "granite-like" bodies in the case of large degrees of partial melting. *Tirel et al*. [2004, 2008] demonstrated the importance of granitic plutons as density anomalies at the base of the middle crust in the formation of extensional gneiss

Additional supporting information may be found in the online version of this article.

[1]Department of Geological and Environmental Sciences, Stanford University, Stanford, California, USA.
[2]WiscSIMS, Department of Geoscience, University of Wisconsin, Madison, Wisconsin, USA.
[3]School of the Environment, Washington State University, Pullman, Washington, USA.
[4]U.S. Geological Survey, Menlo Park, California, USA.

Corresponding author: A. Konstantinou, Department of Geological and Environmental Sciences, Stanford University, Stanford, CA 94305, USA. (akonstan@stanford.edu)

0278-7407/13/10.1002/tect.20085

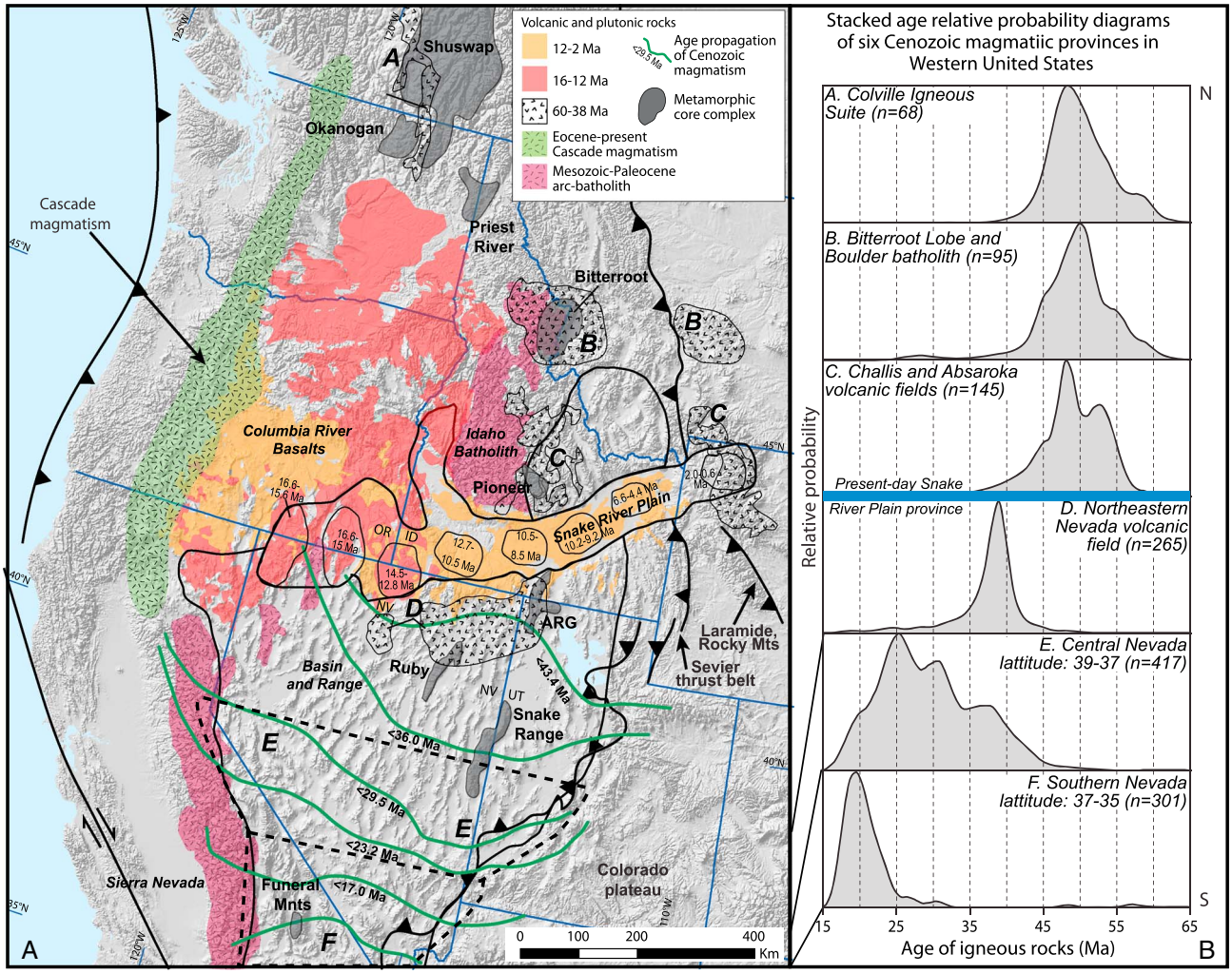

Figure 1. (a) Shaded relief map of the western United States highlighting the Basin and Range and exposures of magmatic rocks of Mesozoic and Cenozoic age. Locations of metamorphic core complexes are shown in dark grey, and the green lines indicate the southward propagation of early-middle Cenozoic magmatism. Letters next and within the areas of Cenozoic magmatism correspond to the relative probability diagrams in Figure 1b. (b) Relative probability diagrams of the ages of Cenozoic (60–18 Ma) igneous rocks from six major magmatic fields in western U.S., compiled from the "NAVDAT" database, excluding altered rocks (based on geochemistry) and excluding rocks with reported ages with more than 5% (1σ) error (see Appendix I in the supporting information). For graph A, the Colville igneous suite spans ~60–40 Ma, with most of the reported ages concentrated between 45 and 52 Ma. In the region of the Bitterroot metamorphic core complex and Boulder batholith (graph B), the ages of Cenozoic igneous rocks span 45–55 Ma, similar to graphs A and C. Ages of the igneous rocks in the Challis and Absaroka volcanic fields (graph C) [*Bennett*, 1986; *Kiilsgaard et al*., 1986]. Between ~41°N and 39°N latitude (the approximate area of northeastern Nevada volcanic field, graph D), magmatism was active from ~45 Ma until ~33 Ma, with most of the reported geochronology results in the time interval 42–37 Ma. The reported ages for igneous rocks in central Nevada (latitude 39–37°N) range from 40 to 20 Ma (graph E). In southern Nevada (latitude 37–35°N), the reported ages of igneous rocks range from 30 to 18 Ma, with most of the data falling between 27 and 20 Ma (graph F).

domes. None of these models, however, discuss the possibility of mass transfer of magma from the mantle into the crust, nor do they address the petrogenesis of the granitic bodies. Studies that focus on magmatism in extensional provinces like the northern Basin and Range [*Gans et al*., 1989] and in the Bering Strait region of Alaska [*Amato et al*., 1994, 2002; *Amato and Miller*, 2004; *Akinin et al*., 2009] alternatively conclude that mantle-derived magmatism is essential to partial melting, remobilization, and flow of crust in extensional settings. In the Bering Strait region, mantle-derived magmatism resulted in both the thermomechanical weakening of the crust and the diapiric rise of magmas that are enveloped in gneissic, high-strain metamorphic carapaces [*Miller et al*., 1992; *Amato and Miller*, 2004]. During this process, stretching and flow of the lower crust results in a sharp subhorizontal Moho and enhanced lower crustal reflectivity [*Klemperer et al*., 2002; *Amato et al*., 2002; *Akinin et al*., 2009]. The plutonic rocks both within and proximal

to metamorphic core complex/gneiss domes described in these two regions are the result of regional magmatism ultimately related to mantle- and lithospheric-scale processes (e.g., slab foundering and slab rollback) rather than just crustal melting associated with overthickening of the crust. Thus, a deeper knowledge of the origin of magmas associated with metamorphic core complexes and gneiss domes is critical to understanding the role of deeper lithospheric processes as drivers for their formation.

[4] This paper focuses on the Eocene to Oligocene magmatic history of the Albion–Raft River–Grouse Creek (ARG) metamorphic core complex as a case study to address the role of magmatism in the structural evolution of a Cordilleran metamorphic core complex. We present new geochronologic data (U-Pb zircon ages), whole-rock geochemical data (major and trace element data and Sr and Nd isotopes), and zircon geochemistry (in situ O-isotope, Hf-isotope, and trace element compositions) from Eocene and Oligocene magmas exposed at three different structural levels, including volcanic rocks erupted at the surface, plutonic rocks intruded into the upper crust (5–8 km), and plutonic rocks intruded at ~12–15 km depths. We evaluate the geochemical evolution of these magmas through time and assess their temporal and compositional links to magmatism, metamorphism, and crustal melting at the more regional scale and their role in the development of gneiss domes and implied lower and middle crustal flow beneath the region of the ARG.

[5] Our results are consistent with Eocene mantle-derived magmatism being the driving mechanism for deep crustal melting with increasing assimilation of crust in the Cenozoic magmas through time. By Oligocene times, this mantle-derived magmatic event resulted in widespread deep crustal melting that weakened the crust, causing it to flow and plutons to rise, ultimately forming the extensional granite-cored gneiss domes of the ARG.

2. Regional Geologic Setting

[6] The northern Basin and Range Province of the western U.S. (Figure 1a) is a broad, active continental rift that is characterized by northerly trending normal fault blocks formed by E-W extension. It is the end product of a protracted history of both magmatism and deformation whose details remain controversial [e.g., *Wernicke*, 1992; *Dickinson*, 2002; *Henry et al*., 2011]. Seismic studies of the northern Basin and Range have shown that at depth, the middle and lower crust is characterized by subhorizontal seismic reflectivity and a sharp and uniform Moho depth of 28–32 km [e.g., *Klemperer et al*., 1986; *Hauser et al*., 1987; *Hauge et al*., 1987; *Catchings and Mooney*, 1991; *Holbrook et al*., 1991; *Catchings*, 1992; *Gashawbeza et al*., 2008]. Its rich history of Cenozoic magmatism has been the subject of many studies. Following the end of regional folding and thrust faulting in the Cretaceous through the earliest Cenozoic (Sevier and Laramide orogenies) [e.g., *Armstrong*, 1982; *Burchfiel et al*., 1992; *DeCelles*, 1994; *DeCelles et al*., 1995; *DeCelles and Coogan*, 2006], Cenozoic volcanic rocks erupted across the region that was to become the future Basin and Range province [e.g., *Christiansen and Lipman*, 1972; *Stewart et al*., 1977; *Gans et al*., 1989; *Armstrong and Ward*, 1991; *Best and Christiansen*, 1991; *Christiansen and Yeats*, 1992; *Axen et al*., 1993; *Christiansen and McCurry*, 2008] (Figures 1a and 1b). The initiation of magmatism began in southern Canada, northern Idaho, and Montana at ~60 Ma and migrated to southern Nevada by ~21 Ma [*Armstrong and Ward*, 1991; *Best and Christiansen*, 1991; *Christiansen and Yeats*, 1992; *Axen et al*., 1993] (Figures 1a and 1b) and has been called the "ignimbrite flare-up" in central Nevada [*Best and Christiansen*, 1991; *Christiansen and Yeats*, 1992].

[7] In order to compare the suite of igneous rock ages from the ARG obtained by this study and by *Strickland et al*. [2011a, 2011b] to magmatism at the regional scale, we utilized data from North American Volcanic and Intrusive Rock Database (NAVDAT), exported on 3 October 2011 [*North American Volcanic and Intrusive Rock Database (NAVDAT)*, 2011]. In order to produce the magmatic age contours and age probability diagrams shown in Figure 1, we incorporated data from both volcanic and plutonic rocks from the Sevier thrust belt on the east to the Cascades and Sierra Nevada on the west (longitude 121°W–110°W) and from southern British Columbia to southern Nevada (latitude 48.5°N–35°N) across the time span 60–18 Ma (selection criteria and methods are described in Appendix I in the supporting information). The NAVDAT data illustrate the southward migration of magmatism from northern Idaho to southern Nevada, as first documented and discussed by *Christiansen and Lipman* [1972], *Stewart et al*. [1977], *Armstrong and Ward* [1991], *Best and Christiansen* [1991], *Christiansen and Yeats* [1992], and *Axen et al*. [1993].

[8] In the region north of the Snake River Plain, Cenozoic magmatism has been interpreted to reflect adakitic magmatism above a slab window or a tear of the Farallon subducting slab [*Breitsprecher et al*., 2003; *Ickert et al*., 2009] (Figure 1). In the region south of the Snake River Plain, Cenozoic magmatism has been attributed to the progressive removal of the Farallon slab [e.g., *Armstrong and Ward*, 1991; *Humphreys*, 1995], which resulted in upwelling of asthenosphere and melting of subduction-hydrated lithospheric mantle [e.g., *Humphreys et al*., 2003; *Lee*, 2005, 2006] (Figure 1).

3. The Albion–Raft River–Grouse Creek Metamorphic Core Complex

3.1. Cenozoic Extensional Deformation in the ARG

[9] The Albion–Raft River–Grouse Creek (ARG) metamorphic core complex is located in southern Idaho and northwestern Utah, ~180 west of the eastern front of the Sevier thrust belt and bound on the north by the Snake River Plain (Figures 1 and 2). The structurally deepest and oldest rocks exposed in the ARG are Archean crystalline rocks of the Green Creek Complex composed primarily of augen orthogneiss with lesser amphibolite, diorite, tonalite, and metasedimentary rocks. These Archean rocks are unconformably overlain by Neoproterozoic quartzites and metapelites that represent the base of the passive margin succession deposited across the northern Great Basin (Figure 2) [*Armstrong*, 1968a; *Compton*, 1972, 1975; *Compton et al*., 1977; *Stewart*, 1980]. Higher stratigraphic units include Phanerozoic (Ordovician through Cenozoic) unmetamorphosed to weakly metamorphosed sedimentary rocks [e.g., *Compton et al*., 1977] (Figure 2). Based on stratigraphic considerations alone, the relative uplift of rocks in the ARG compared to surrounding regions that expose supracrustal sedimentary and volcanic

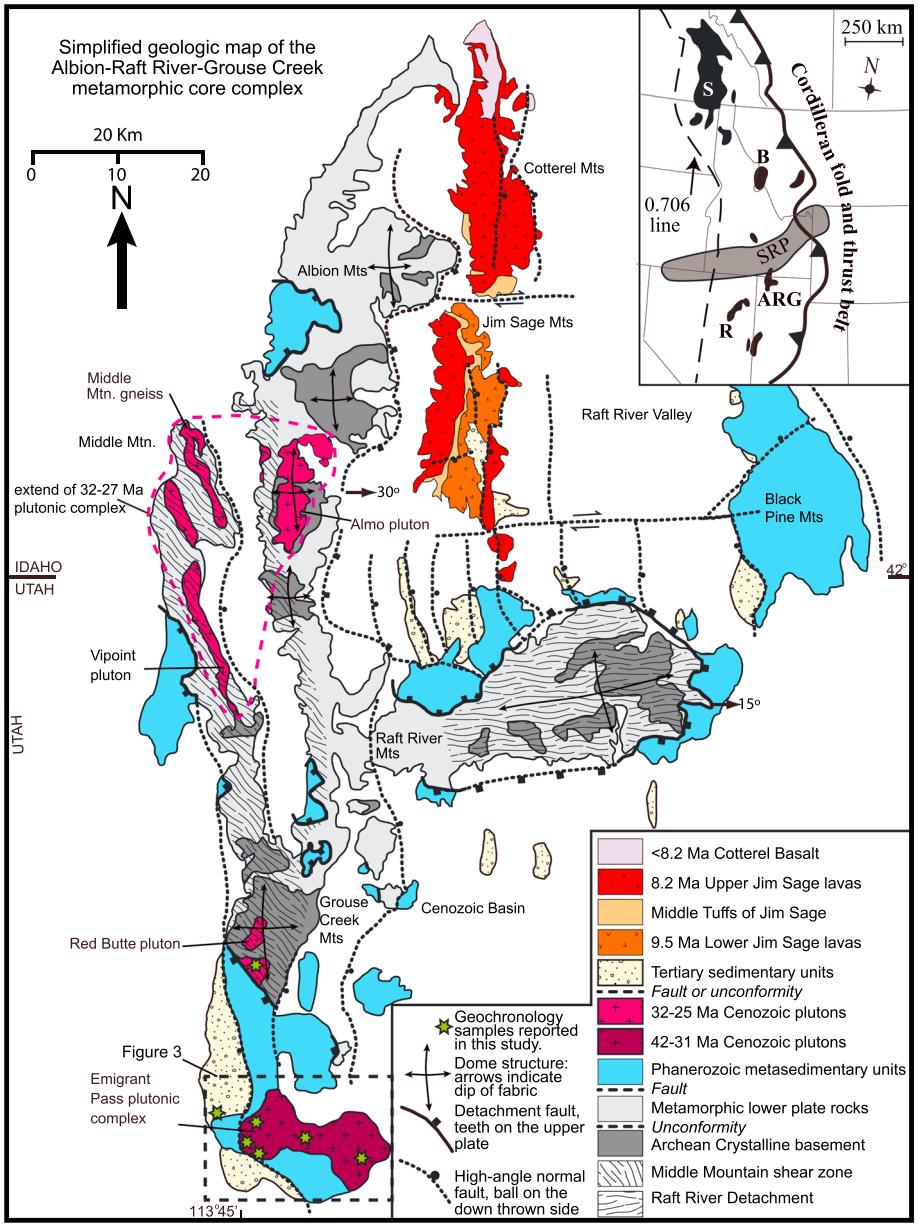

Figure 2. Generalized geologic map of the Albion–Grouse Creek–Raft River Mountains. Dashed line indicates the location of Figure 3. Modified from *Compton* [1972, 1975], *Miller* [1978], *Todd* [1980], *Miller et al*. [2008], *Wells* [2009], and *Strickland et al*. [2011b]. The inset map shows the location of the ARG in the western Cordillera.

sequences is a minimum of ~10 km [*Compton et al*., 1977; *Stewart*, 1980].

[10] The first detailed studies of the ARG metamorphic core complex were those of *Armstrong* [1963, 1968b] and *Armstrong and Hills* [1967], who suggested that it represented a series of mantled gneiss domes (Figure 2) that formed partly in Oligocene times during the intrusion of granitic plutons, a view that was further elaborated upon by later workers [*Compton et al*., 1977; *Miller*, 1980; *Todd*, 1980; *Miller*, 1983]. The gneiss domes are defined by metamorphic foliation, and their emplacement or formation has been inferred to be the result of extreme strain, attenuation, and stretching of the middle crust, which resulted in horizontal to gently dipping foliations and NW-SE to E-W lineations (L-S tectonites) that involve the tops and western borders of Oligocene granitic plutons [*Armstrong*, 1968; *Compton et al*., 1977; *Todd*, 1980; *Armstrong*, 1982; *Saltzer and Hodges*, 1998; *Sullivan*, 2008; *Strickland et al*., 2011a, 2011b; *Konstantinou et al*., 2012]. Many studies have demonstrated a Cretaceous history of metamorphism in the ARG [e.g., *Armstrong*, 1968b; *Wells et al*., 2012], which has been interpreted to reflect alternating episodes of contraction and extension in the western U.S. during the Mesozoic [e.g., *Wells et al*., 2012, and references therein]. Cenozoic fabrics have overprinted much of this Cretaceous fabric, making the study and interpretation of the Cretaceous history of the complex more difficult to decipher than its Cenozoic history [e.g., *Miller et al*., 2012]

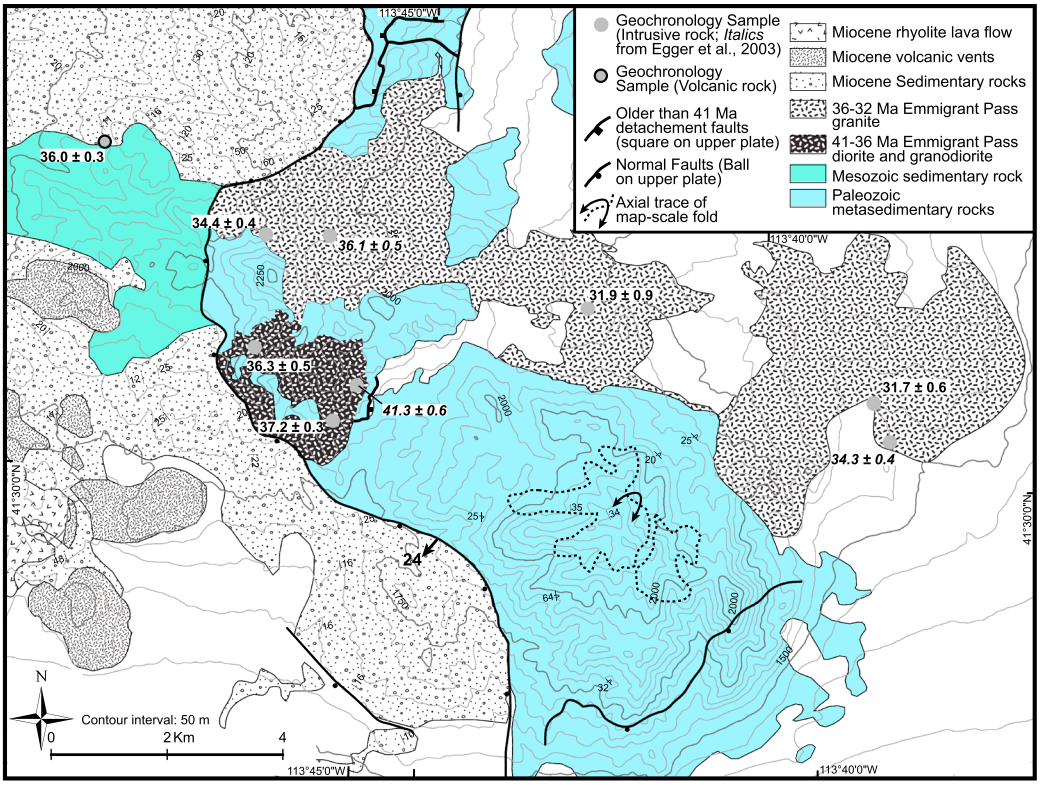

Figure 3. Generalized map of the southern Grouse Creek mountains, showing the extent of the Emigrant Pass plutonic complex (EPC). The locations and geochronology results from this study and *Egger et al.* [2003] are in italics. Modified from *Egger et al.* [2003].

[11] Recent geochronologic studies of metamorphic and plutonic rocks from the Albion and Middle Mountains have supported the conclusions of earlier workers in that much of the Cenozoic deformation in the core complex may be explained as related to the formation of a series of granite-cored gneiss domes that formed episodically during late Eocene and Oligocene times (~34–25 Ma; Figure 2) [*Strickland et al.*, 2011a, 2011b; *Konstantinou et al.*, 2012]. These interpretations are supported by geologic mapping, field relationships, structural and microstructural studies, and the geochronology of igneous and metamorphic rocks.

[12] *Strickland et al.* [2011a] illustrated that extreme thinning of the Paleozoic section from ~1500 m in the Raft River Mountains to 350 m in the southern Middle Mountain, and the development of subhorizontal high-strain foliations and NW-SE stretching lineations at amphibolite facies, is spatially associated with the intrusion of the Vipoint pluton (Figure 2). This metamorphic fabric, which overprints an earlier Cretaceous metamorphic event [e.g., *Wells et al.*, 2012], was dated by U-Pb geochronology of monazite from metamorphic rocks and pegmatites boudinaged within the foliation as forming between 32 and 27 Ma. Approximately 20 km north of the Vipoint pluton, subhorizontal foliation and NW-SE stretching lineation deform the Middle Mountain orthogneiss, a calc-alkaline pluton dated by U-Pb geochronology at 32.1 ± 0.6 to 31.8 ± 0.4 Ma (Figure 2) [*Strickland et al.*, 2011b]. In the Albion Mountains and the northern Middle Mountains, the high-strain foliation and well-developed NW-SE stretching lineation are defined in part by sillimanite growing in asymmetric top-to-the-west shear bands, and a series of strain-collapsed isograds have been mapped on top and around the gneiss domes and the western and northern part of the Almo pluton dated between 30.6 ± 0.3 and 28.9 ± 0.3 Ma using zircon U-Pb geochronology (Figure 2) [*Strickland et al.*, 2011b; *Konstantinou et al.*, 2012]. This fabric and metamorphism is thought to reflect thinning and flow at amphibolite facies conditions during the development of the gneiss domes. Similar relationships have been documented in the Grouse Creek Mountains, where subhorizontal high-strain foliation and NW-SE stretching lineations involve both the country rocks and the Red Butte pluton, which is dated as ~25 Ma (Figure 2) [*Egger et al.*, 2003; this study].

[13] Collectively, the cross-cutting field relationships and the geochronology of Cenozoic plutons and high-temperature metamorphic rocks illustrate that Oligocene ductile extensional flow and metamorphism accompanied plutonism in the ARG. Deformation is focused along the top of the western side of the Almo pluton and in the top-to-the-NW Middle Mountain shear zone [e.g., *Saltzer and Hodges*, 1998; *Sullivan*, 2008; *Strickland et al.*, 2011a, 2011b] (Figure 2) and collectively occurred mostly between ~34 and 25 Ma. A more detailed account of the field relationships in the lower plate of the ARG and their relationship to the emplacement of the Cenozoic plutons can be found in *Egger et al.* [2003], *Strickland et al.* [2011a, 2011b], and *Konstantinou et al.* [2012]. Alternative views propose that the 34–25 Ma magmatism is unrelated (and younger) than the main extensional deformational and metamorphism in

Table 1. Summary Information of Samples From This Study[a]

Sample Number	Age	Unit	Type of Analysis	Description	Coordinates (Deg. Dec. Deg.) N	Coordinates (Deg. Dec. Deg.) W	Elevation (m)	Weighted Mean $^{206}Pb/^{238}U$ Youngest Age (Depositional Age) With Error		Mean $\delta^{18}O$ VSMOW, ‰	Mean $\varepsilon_{Hf(i)}$
AL-1	Oligocene	CPC; Almo pluton	MT	mafic enclave of granite	42.04228	113.71797	1923	Not determined	--	--	--
GC-1	Eocene	SW phase of EPC	MT, O, Hf, GT	ignimbirte	41.54974	113.80434	1833	36.0	±0.3	6.67 ± 0.11	−17.1 ± 0.4
GC-4	Eocene	SW phase of EPC	MT, WI	microdiorite	41.51975	113.77303	2045	Not determined	--	--	--
GC-5A	Eocene	SW phase of EPC	MT, WI, O, Hf, GT	monzogabbro	41.51847	113.77289	2042	Not determined	--	--	--
GC-5B	Eocene	SW phase of EPC	MT, O, GT	monzogabbro	41.51847	113.77289	2042	36.3	±0.5	6.26 ± 0.16	−25.9 ± 0.5
GC-5C	Eocene	SW phase of EPC	MT, WI, O, Hf, GT	diorite	41.51847	113.77289	2042	Not determined	--	--	--
TEP	Eocene	NE phase of EPC	MT, WI	granite	41.53157	113.68903	1703	Not determined	--	--	--
TEP-1	Oligocene	NE phase of EPC	MT, O, Hf, GT	granite	42.52493	113.70081		31.9	±0.9	4.81 ± 0.12	−28.9 ± 2.1
TEP-2	Eocene	SW phase of EPC	MT, WI, O, Hf, GT	diorite	41.50781	113.64261		37.2	±0.3	5.92 ± 0.12	−21.7 ± 1.5
TEP-5	Eocene?	NE phase of EPC	MT	granite	41.52664	113.66625		Not determined	--	--	--
TEP-7	Oligocene	NE phase of EPC	MT, WI, O, Hf, GT	granite	41.50871	113.64261		31.7	±0.6	4.90 ± 0.08	−31.2 ± 3.6
TEP-9	Eocene	NE phase of EPC	MT, O, Hf, GT	granite	41.53638	113.76780		34.4	±0.5	5.06 ± 0.08	−26.8 ± 0.3
TEP-10	Eocene?	NE phase of EPC	MT	granite	41.52027	113.65798		Not determined	--	--	--
TRB	Oligocene	CPC; Red butte pluton	MT, WI, O, Hf, GT	granite	41.67488	113.75541		24.5	±0.4	5.11 ± 0.11	−34.6 ± 1.7
RR-5A	?	Archean basement	MT, WI	amphibolite	41.95603	113.32514		Not determined	--	--	--
RR-5B	?	Archean basement	MT, WI	amphibolite	41.95603	113.32514		Not determined	--	--	--
RR-7	?	Archean basement	MT, WI	tonalite	41.95639	113.31242	1904	Not determined	--	--	--

MT = Major and trace elements; WI = whole-rock Sr and Nd isotopes; O = zircon oxygen isotope; Hf = zircon Hf isotope; GT = zircon geochronology and zircon trace element.
[a]Coordinates reported in the North American Datum of 1983.

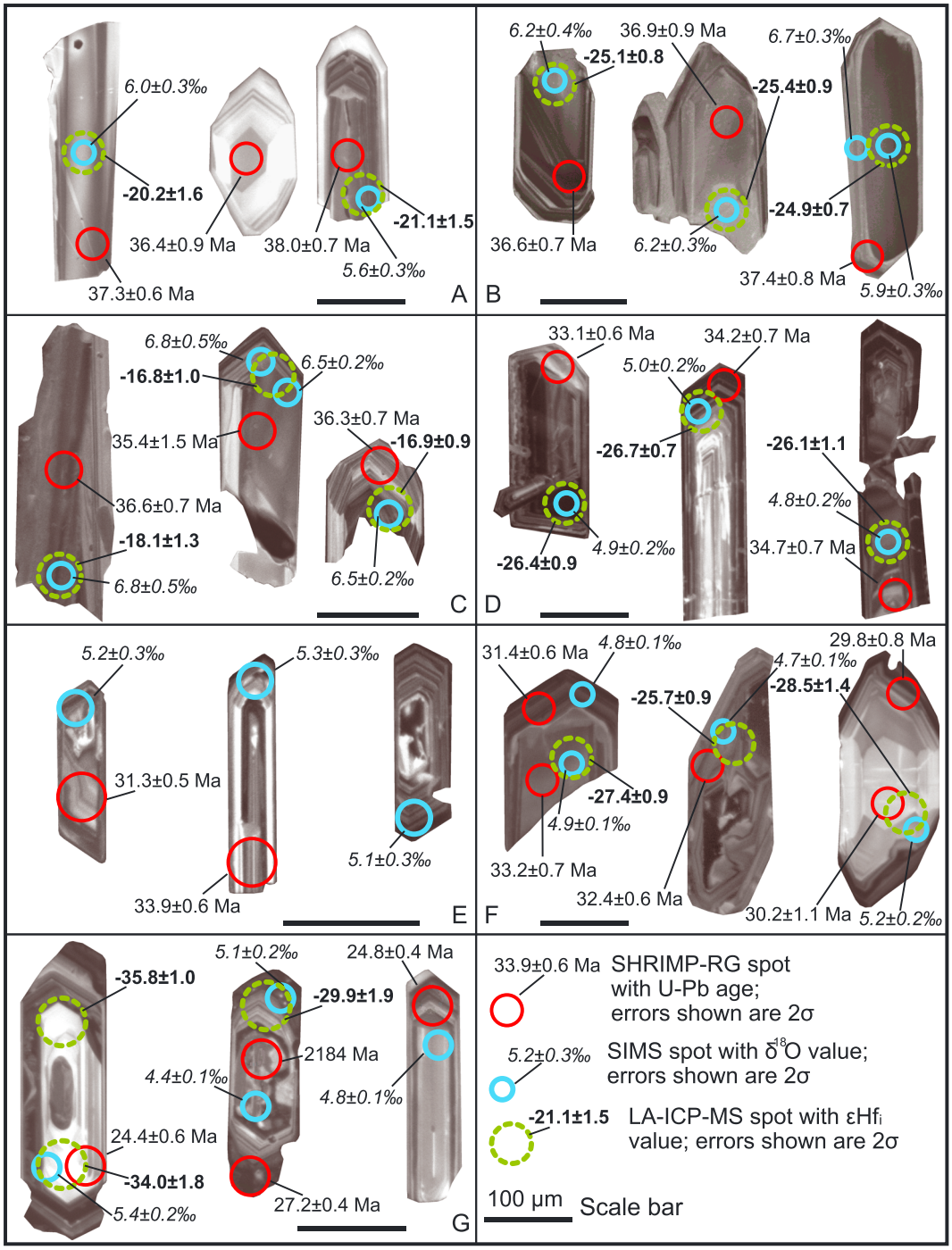

Figure 4. Diagram showing representative cathodoluminescence images of zircons from the igneous rocks dated in this study. Samples: A = TEP-2; B = GC-5B; C = GC-1; D = TEP-9; E = TEP-1; F = TEP-7; G = TRB. Red circles indicate the spots where ^{207}Pb-corrected ^{206}Pb/^{238}U ages were obtained from SHRIMP-RG analyses, blue circles indicate the spots analyzed for O isotope ratios by SIMS, and green circles indicate spot locations from Hf isotope analyses by LA-ICP-MS. The scale bar is 100 µm for all the samples.

the complex, as constrained by the growth of monazite in garnets and ^{40}Ar/^{39}Ar thermal histories [e.g., *Wells et al.*, 2000, 2012].

[14] The final exhumation of the granite-cored gneiss domes of the ARG metamorphic core complex was accomplished by large-offset (~10 km) high-angle normal faults and rolling-hinge-type extensional detachment faults (such as the Raft River detachment) during the Miocene (15–7 Ma) [*Compton*, 1983; *Wells et al.*, 2000; *Egger et al.*, 2003; *Konstantinou et al.*, 2012], with extreme transient geothermal gradient locally documented and inferred to be related to convective flow of surface waters [*Gottardi et al.*, 2011]. These structures are significantly younger than the gneiss dome phase of core complex development in the

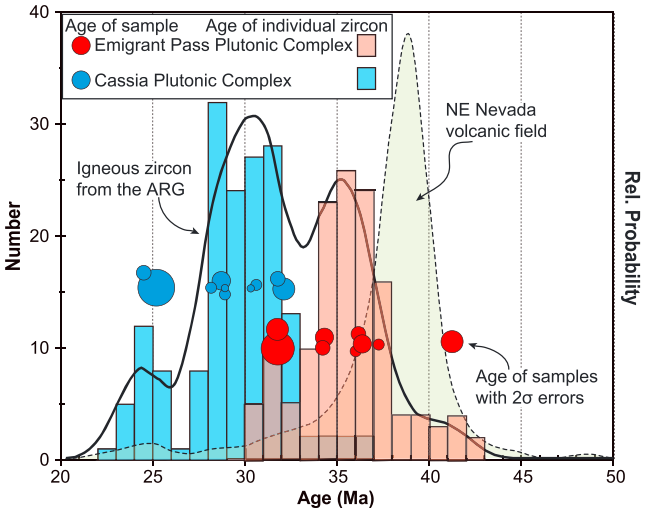

Figure 5. Relative probability diagram and histogram of the zircon ages from Cenozoic plutons determined from the ARG (including data from *Egger et al*. [2003] and *Strickland et al*. [2011b]). Note the overlap in ages of the Emigrant Pass plutonic complex (EPC) and the Cassia plutonic complex (CPC). Red circles indicate the ages and 2σ errors of individual samples from the EPC, while blue circles indicate the ages and 2σ errors of samples from the CPC. The probability curve of the northern Nevada volcanic field is also shown for comparison.

ARG and are partly coeval with Miocene Snake River Plain magmatism [*Konstantinou*, 2011; *Konstantinou et al*., 2012].

3.2. Magmatism in the ARG

[15] Cenozoic igneous rocks are exposed both within and flanking the ARG metamorphic core complex (Figure 2) and were erupted or intruded during three distinct events in the late Eocene, the Oligocene, and the late Miocene. During the late Eocene (41–32 Ma), the calc-alkaline intermediate to felsic Emigrant Pass plutonic complex (EPC) was emplaced at shallow crustal levels (5–8 km), based on the growth of metamorphic minerals that include andalusite in the immediate contact aureole of the pluton [*Compton*, 1977; *Egger et al*., 2003; Figures 2 and 3]. The EPC is elongated in an E-W direction and has an approximate aerial extent of ~75 km^2 (Figure 3), but it is probably broader at depth considering its inferred exposure beneath thin quaternary deposits and its gravity and magnetic anomalies [*Khattab*, 1969; *Langenheim et al*., 2011]. The plutonic complex is divided into a diorite phase with mafic dikes along its southwestern edge (SW EPC) and a granitic phase with garnet-bearing aplite dikes on its northeastern side (NE EPC) [*Egger et al*., 2003; *Compton*, 1977; *Baker*, 1959] (Figure 3). Eocene volcanic rocks of dacitic-rhyolitic composition—possibly volcanic counterparts to the plutonic complex—were first mapped by *Compton* [1983]. A crystal-rich vitric tuff near the base of the Cenozoic sedimentary section along the western side of the Grouse Creek Mountains (in fault contact with the plutonic rocks, Figure 3) yielded a K-Ar biotite age of 36.4 ± 1.1 Ma, and K-Ar analysis of sanidine from an ashfall tuff slightly higher in the section produced an average age of 33.4 ± 1.0 Ma [*Compton*, 1983]. These volcanic rocks are within the age range of the Emigrant Pass plutonic complex, and their link to the plutonic complex is discussed in this study.

[16] During the Oligocene, magmatism in the ARG metamorphic core complex is represented by the Cassia plutonic complex (CPC) [*Strickland et al*., 2011b]. The CPC appears to have limited map extent (Figure 2) because it is dissected by normal faults and covered by basin fill. Geologic cross sections together with geochronology show that the complex underlies an extensive region of the ARG (Figure 2, shown by red line) [*Egger et al*., 2003; *Strickland et al*., 2011b]. The Oligocene plutonic complex intruded country rocks as they experienced amphibolite facies conditions (~3.5–4 kbar; 650°C) [*Egger et al*., 2003; *Strickland et al*., 2011a, 2011b; *Konstantinou et al*., 2012], and parts of it are involved in the high-strain foliation and NW-SE extensional stretching fabrics. The oldest pluton in the CPC is the Middle Mountain orthogneiss, dated at 32 Ma [*Strickland et al*., 2011b], and for the purpose of this study, we include the younger Red Butte pluton in the Grouse Creek Mountains dated at ~25 Ma as part of the CPC [*Compton et al*., 1977; *Todd*, 1980; *Egger et al*., 2003; this study] (Figure 1). There is no evidence that the studied plutons in the 32–25 Ma age range had volcanic equivalents. Miocene (14–8 Ma) volcanic rocks are present adjacent to the metamorphic core complex (Figure 1) but are not the subject of this paper.

4. Methods

[17] Single-grain zircon U-Pb analyses ($n = 168$) from seven samples were carried out using the sensitive high-resolution ion microprobe reverse geometry (SHRIMP-RG) at the Stanford-USGS facility. Five samples were collected from the Emigrant Pass plutonic complex (two from the SW phase and three from the NE phase), one sample from a vitric tuff deposited unconformably above Triassic sedimentary rocks in the hanging wall of the Miocene Grouse Creek Fault [*Martinez*, 2000; *Egger et al*., 2003], and one from the Red Butte pluton (Table 1 and Figures 4 and 5). Detailed methods and description of the results are in Appendix I in the supporting information.

[18] Sixteen samples were analyzed for whole-rock geochemistry (see details and results in Appendix II in the supporting information). Five samples are from the SW phase of the Emigrant Pass plutonic complex, six samples are from the NE phase, two samples are from the Oligocene Cassia plutonic complex, and three samples are from Archean crystalline rocks (Table 1 and Appendix II in the supporting information).

[19] Nine samples were selected for whole-rock Sr and Nd analyses performed at the Stanford MC-ICP-MS facility (Table 1 and Appendix III in the supporting information). Six samples are from the SW phase of the Emigrant Pass plutonic complex, two are from the NE phase, one is from the Oligocene Red Butte pluton, and one amphibolite is from the Archean crystalline basement exposed in the ARG. The procedures used are sample dissolution and mass spectrometry, and the results are found in Appendix III in the supporting information.

[20] Zircon trace element compositions of the seven dated samples described above were determined by in situ analyses using the SHRIMP-RG. The description of the procedure and

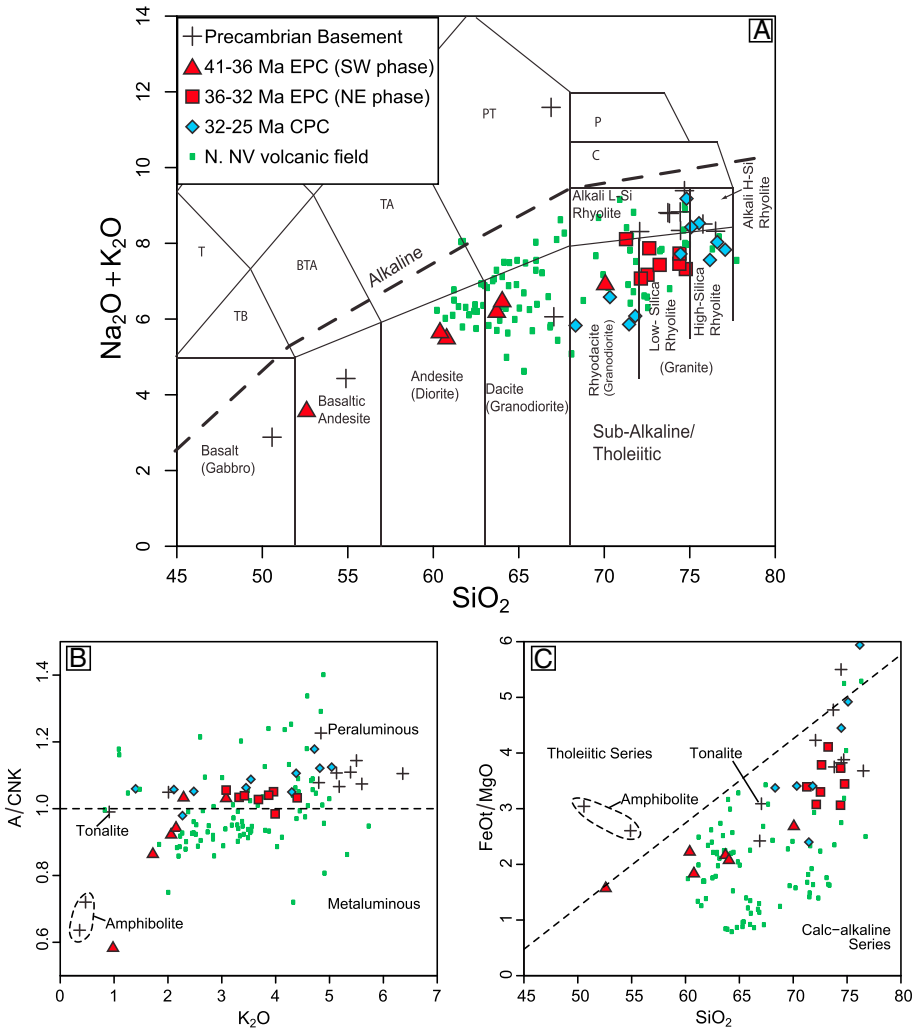

Figure 6. Whole-rock major element compositions of samples from the EPC, CPC, Precambrian igneous rocks, and the northeastern Nevada volcanic field. Key is the same for Figures 6a–6c. (a) Total alkali versus silica (TAS) diagram indicating the range of compositions of the Precambrian basement, the SW and NE phases of the Emigrant Pass plutonic complex (EPC), the Cassia plutonic complex (CPC), and the northeastern Nevada volcanic field. (b) Alumina/$CaO + Na_2O + K_2O$ (A/CNK) versus K_2O. (c) FeOt/MgO versus SiO_2 diagrams of the same suite of rocks.

the results are found in Appendix IV in the supporting information. The O-isotope composition of zircon from seven Cenozoic samples (Table 1 and Figure 4; $n = 168$) was determined in situ using an IMS-1280 at the WiscSIMS facility following the procedures described in *Kita et al.* [2009] and *Valley and Kita* [2009], and $\delta^{18}O$ [Vienna SMOW (VSMOW)] values were calculated at the 2σ level (see Appendix V in the supporting information for details of the method and the results). For the purpose of this study, we have used the $\delta^{18}O_{zr}$ values to calculate $\delta^{18}O_{wr}$ using the equation rearranged from *Lackey et al.* [2008], i.e.,

$$\delta^{18}O_{wr} \approx \delta^{18}O_{zr} + 0.0612\,(\mathrm{wt\%SiO_2}) - 2.5$$

[21] Hf-isotopic compositions were determined in situ on zircon grains from nine Cenozoic samples (Table 1) at Washington State University's LA-MC-ICP-MS facility using the procedure described in *Fisher et al.* [in review] (Table 1 and Figure 4). Five Oligocene samples with inherited cores and Cenozoic rims were analyzed using a split-stream geometry (Appendix VI in the supporting information). The $^{176}Hf/^{177}Hf$ and $^{176}Lu/^{177}Hf$ ratios and the SHRIMP-RG sample ages were used to calculate $\varepsilon_{Hf(o)}$ and $\varepsilon_{Hf(t)}$ values reported in Appendix VI in the supporting information.

5. Results and Interpretation

5.1. In Situ Zircon SHRIMP-RG U-Pb Geochronology

[22] The geochronologic results from this study add to those of *Strickland et al.* [2011b] from the igneous rocks of the Cassia plutonic complex and those of *Egger et al.* [2003] from the Emigrant Pass plutonic complex and are summarized in Figure 5. The collective data from the EPC reported in this study and by *Egger et al.* [2003] indicate that magmatism spanned from 41 Ma to 32 Ma. The SW phase of the complex is the oldest, as first documented by *Compton et al.* [1977], and ranges in age from 41 to 36 Ma. Zircon

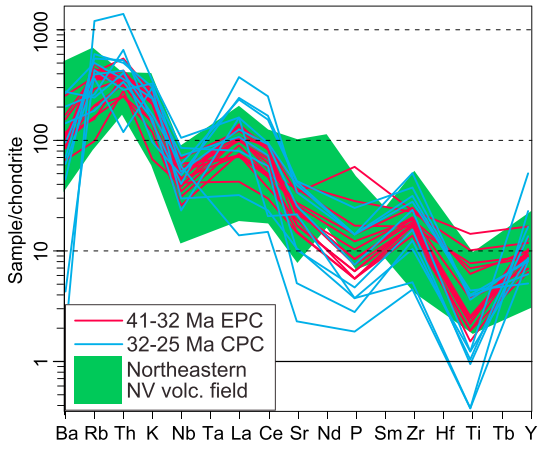

Figure 7. Whole-rock chondrite-normalized spider diagram of trace elements of samples from the Emigrant Pass complex (EPC), the Cassia plutonic complex (CPC), and the northeastern Nevada volcanic field.

from this phase lack inherited zircon cores (Figures 4a–4c). The NE phase is younger, ranging from ~35 to 32 Ma, and its zircon crystals have abundant inherited cores (Figures 4d–4g). The data from the EPC and the Cassia plutonic complex (CPC, including the Red Butte pluton) indicate nearly continuous crystallization of magmatic zircon from ~41 to 25 Ma, with a slight overlap in the ages of the Emigrant Pass plutonic complex (EPC, 41–32 Ma) and the Cassia plutonic Complex (CPC, 32–25 Ma; Figure 5).

[23] The age of crystallization of the EPC overlaps with the reported ages of (mostly) volcanic rocks in the northeastern Nevada volcanic field (Figures 1 and 5). The CPC postdates the age of volcanism documented across northeast Nevada; in fact, its intrusion spans a period of noted volcanic quiescence across the northernmost Basin and Range [e.g., *Armstrong and Ward*, 1991; *Burton*, 1997; this study] (Figure 1b).

5.2. Major and Trace Element Geochemistry

[24] Major and trace element analyses performed in this study together with results from 9 Archean and 12 Cenozoic igneous rock samples were included in the data shown in Figures 6 and 7 (compiled from *Egger et al.* [2003] and *Strickland et al.* [2011b]). Data from the northeastern Nevada volcanic field are from *Brooks et al.* [1995] and *NAVDAT* [2011]. The Emigrant Pass plutonic complex (EPC) ranges in composition from hornblende monzogabbro ($SiO_2 = 53\%$) through granite ($SiO_2 = 75\%$), and the Cassia plutonic complex (CPC) is composed of granodiorite through high silica granite, but there is a significant overlap in composition between the EPC and the CPC, and the magmas follow a common evolutionary trend (Figure 6). Cenozoic magmas of the ARG are calc-alkaline (Figure 6c) and evolve from metaluminous (A/CNK < 1.0 for the SW phase of the EPC) to weakly peraluminous (A/CNK ~1–1.1 for the NE phase of EPC) and strongly peraluminous (A/CNK > 1.1 for the CPC; Figure 6b). The three plutonic complexes have similar trace element patterns (Figure 7). All samples analyzed have strong enrichments in large-ion lithophile element (LILE) incompatible elements and moderate enrichments in high field strength (HFS) incompatible elements, with Nb and Ti anomalies (Figure 7). The Cenozoic magmas of the ARG, in terms of both their major and trace element compositions, are similar to magmas from the northeastern Nevada volcanic field, which are calc-alkaline and metaluminous to peraluminous andesites to rhyolites, with strong LILE enrichments and Nb and Ti anomalies (Figures 6 and 7).

[25] Previous work by *Strickland et al.* [2011b] suggested that the Archean augen gneiss now exposed in the ARG is unlikely to represent the only crustal source for the CPC because of its highly radiogenic Sr isotopic composition, and they suggested that that intermediate Archean crustal sources might exist at greater depth. In order to better understand the compositional variability of rocks represented by the Archean complex, more rock types from the Archean basement in the Albion and Raft River Mountains were analyzed: a Precambrian tonalite and two amphibolite samples (a metadiorite and a metagabbro). All three samples have metaluminous bulk geochemistry (Figure 6).

5.3. Whole-Rock MC-ICP-MS Sr and Nd Isotope Analyses

[26] Our whole-rock Sr and Nd isotope results, together with isotopic analyses reported in *Strickland et al.* [2011b] and *Wright and Wooden* [1991], were used to calculate age-corrected $^{87}Sr/^{86}Sr_i$ and $\varepsilon_{Nd(i)}$ values (Figure 8). Sr and Nd isotopic values for the Precambrian basement samples were calculated at 40 Ma, rather than the age of the rock, to estimate their isotopic composition at the time of onset of Cenozoic magmatism and to compare with the initial isotopic compositions of the Emigrant Pass plutonic complex (EPC) and the Cassia plutonic complex (CPC; Figure 8). The EPC has initial isotopic compositions of $^{87}Sr/^{86}Sr_i = 0.7089–0.7110$ and $\varepsilon_{Nd(i)}$ values from −16 to −24; the CPC has initial isotopic compositions of $^{87}Sr/^{86}Sr_i = 0.7111–0.7156$ and $\varepsilon_{Nd(i)}$ values from −26.3 to −36.1 (Figure 8). The Precambrian amphibolite sample has a $^{87}Sr/^{86}Sr_{40\ Ma}$ value of 0.717 and an $\varepsilon_{Nd(40\ Ma)}$ value of −24.8 (Figure 8). The Precambrian felsic rocks have a range of isotopic compositions of $^{87}Sr/^{86}Sr_{40\ Ma} = 0.798–1.044$ and $\varepsilon_{Nd(40\ Ma)}$ of −28.2 to −43.4 (Figure 8) [*Strickland et al.*, 2011b].

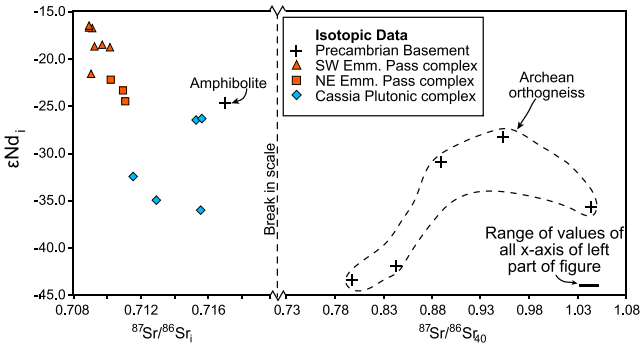

Figure 8. $^{87}Sr/^{86}Sr_i$ versus $\varepsilon_{Nd(i)}$ compositions of samples from the Precambrian basement, the SW and NE phases of the Emigrant Pass complex (EPC), and the Cassia plutonic complex (CPC) in the ARG metamorphic core complex. Data were compiled from *Wright and Wooden* [1991], *Strickland et al.* [2011b], and this study.

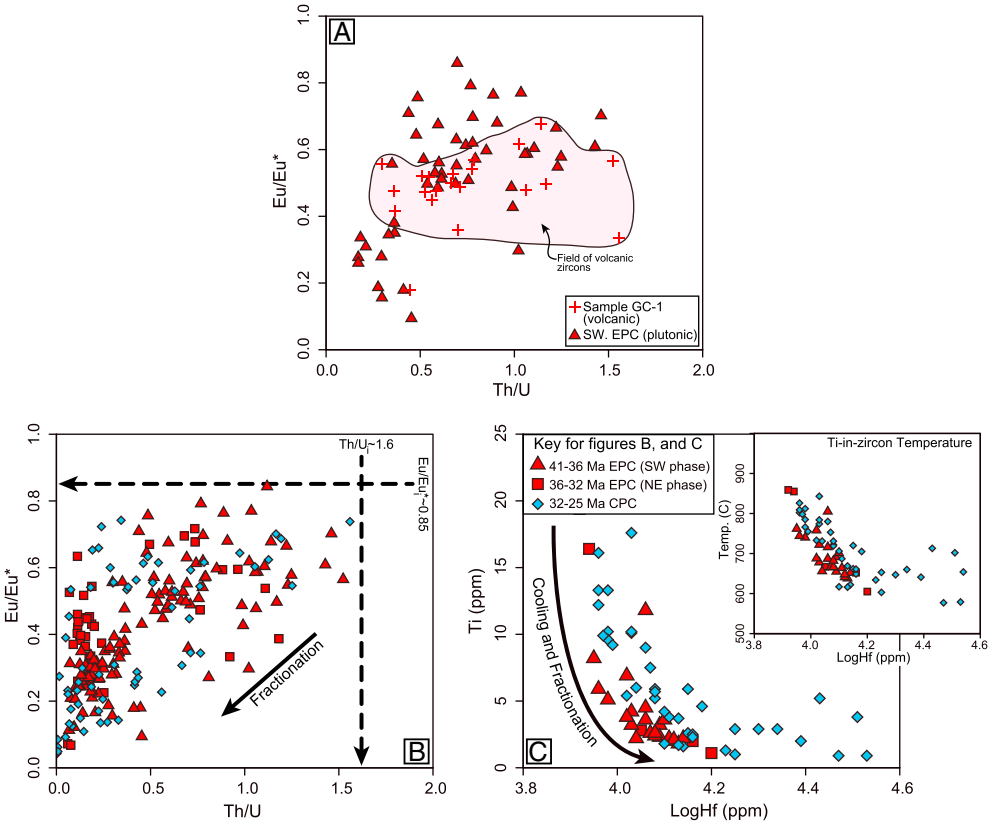

Figure 9. (a) Trace element compositions (Eu/Eu* versus Th/U) of zircons from the SW phase of the Emigrant Pass complex and the volcanic sample from the Grouse Creek Mountains (pink field) indicated the overlap in composition in the two data sets. (b) Trace element compositions (Eu/Eu* versus Th/U) of zircons from the Emigrant Pass complex (EPC) and the Cassia plutonic complex (CPC) showing the decrease in Eu/Eu* and Th/U with fractionation and the "unfractionated" values of Eu/Eu^*_i (~0.85) and Th/U_i (~1.6). (c) Trace element composition [Ti versus log(Hf)] of zircons from the Emigrant Pass complex (EPC) and the Cassia plutonic complex (CPC) showing the decrease of Ti with fractionation. The calculation of the Ti-in-zircon temperature (inset) [*Ferry and Watson*, 2007] assumes $aSiO_2 = 1$, $aTi = 0.7$, and 1 GPa pressure.

5.4. In Situ Zircon SHRIMP-RG Trace Element Geochemistry

[27] The trace element geochemistry of zircon is a useful petrogenetic indicator and reflects the evolution of the magmas from which the zircons crystallized [e.g., *Barth and Wooden*, 2010]. The europium anomaly (Eu/Eu*) in magmas is an indicator of the fractionation of the melt due to the crystallization of plagioclase feldspar and is also a function of the fO_2 in magmas. The Th/U ratios of magmas are also indicators of fractionation, controlled by the crystallization of minor phases such as allanite and zircon.

[28] The 36.1 Ma vitric tuff (GC-1) has similar Eu/Eu* and Th/U ratios to samples from the SW phase of the EPC (Figure 9a). Figures 9b and 9c compare the zircon trace element compositions of the SW phase (red triangles) of the EPC, the NE phase of the EPC (red squares), and the CPC (blue diamonds). The Eu/Eu* versus Th/U plot (Figure 9b) for all dated zircons indicates that the least fractionated zircons have a Eu/Eu^*_i of ~0.85 and a Th/U_i of ~1.6, both of which reflect the least fractionated (mafic) composition of the magmatic system. The Ti versus Hf plot shows similar fractionation trends for the magmas of the EPC and CPC, indicating a record of similar initial elevated magma temperatures reflected by Ti-in-zircon temperatures (Figure 9c).

5.5. In Situ Zircon SIMS O Isotope Analyses

[29] The O-isotope composition of zircons from the seven samples dated yielded weighted average $\delta^{18}O_{zr}$ (VSMOW) in the range 4.8–6.7‰ (Figure 10a, inset; Table 1 and Appendix V in the supporting information). Zircons with ages of 38–35 Ma have O-isotope compositions of $\delta^{18}O_{zr}$ ~5.6‰ to ~6.8‰, which is higher than the weighted average value measured on inherited Precambrian zircon cores ($\delta^{18}O_{zr} = 5.6 \pm 0.2$‰; 2σ) [*Strickland et al.*, 2011b; this study]. Zircons with ages of 35–25 Ma have O-isotope compositions of $\delta^{18}O_{zr}$ from ~5‰ to 6‰ requiring a fairly homogeneous magma reservoir for a prolonged period of time (~10 Ma) (Figure 10a). Moreover, when melt $\delta^{18}O_{wr}$ values are calculated from the measured zircon values (using the equation above) [*Lackey et al.*, 2008], the calculated $\delta^{18}O_{wr}$ values of both the EPC and CPC magmas have a uniform range with ~88% of the calculated $\delta^{18}O_{wr}$ being between 6.5‰ and 7.5‰, with a weighted average value of $\delta^{18}O_{wr} = 7.15 \pm 0.05$‰ (95% confidence level).

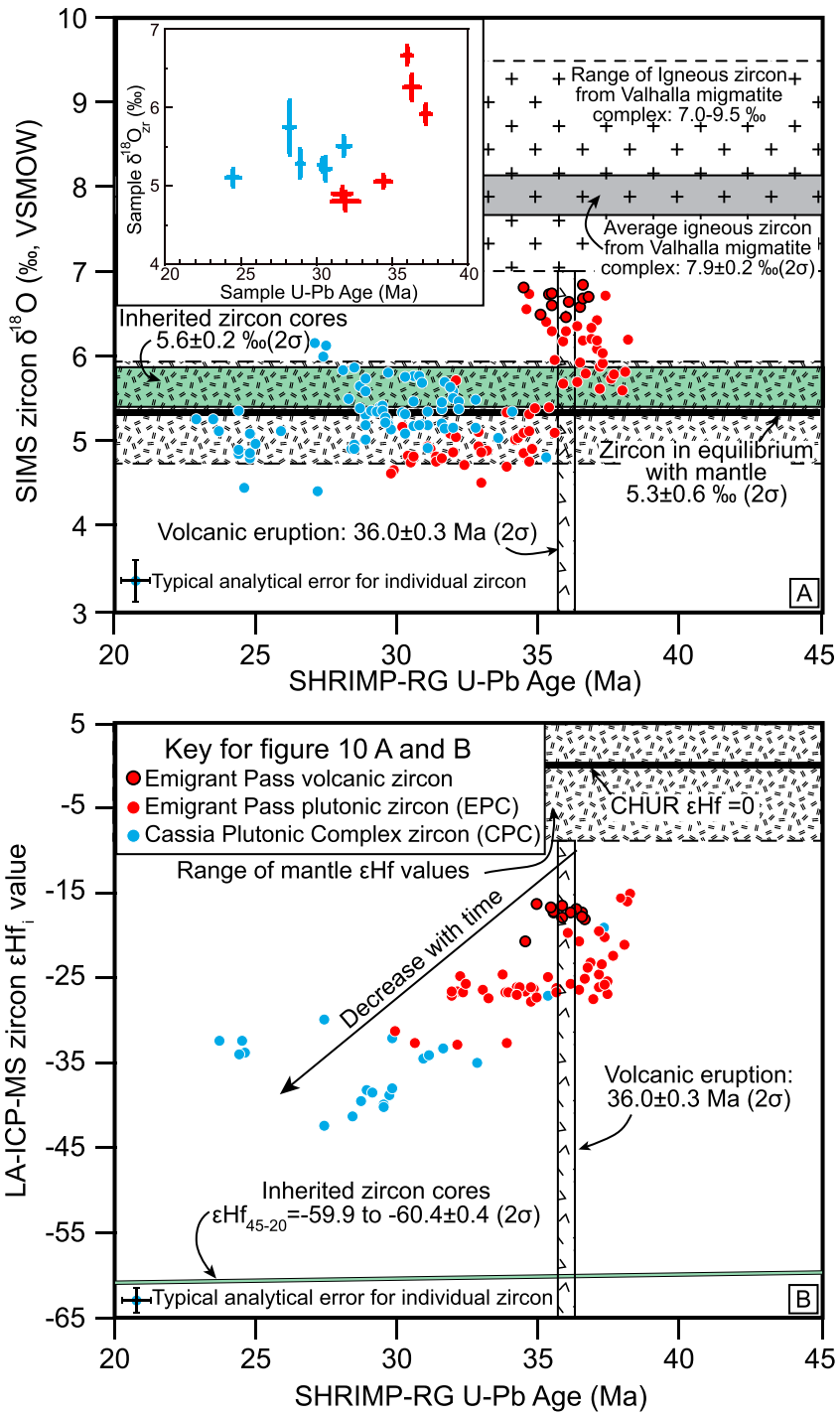

Figure 10. Diagram summarizing the temporal zircon (a) oxygen-isotope ($n = 155$) and (b) Hf-isotope ($n = 114$) compositions from igneous rocks from the ARG. The key in Figure 10b is for both graphs. The inset in Figure 10a shows the weighted average $\delta^{18}O_{zr}$ and U-Pb age of individual samples. Red symbols are for the EPC, and blue symbols are for the CPC. Also shown for comparison are the O-isotope compositions for zircon in equilibrium with the mantle [*Valley*, 2003; *Valley et al.*, 1998], the igneous zircon from the Valhalla migmatite complex [*Gordon et al.*, 2009], and the oxygen- and Hf-isotope compositions of inherited zircon cores from the Cenozoic igneous rocks in the ARG [*Strickland et al.*, 2011b; this study].

[30] When our results from Cenozoic zircon are compared with reported $\delta^{18}O_{zr}$ values of igneous zircon from Cenozoic leucogranites and leucosomes exposed in the Valhalla migmatite complex (average $\delta^{18}O_{zr} = 7.9 \pm 0.2‰$) [*Gordon et al.*, 2009], they are lower by ~1–3‰ (Figure 10a). The high $\delta^{18}O_{zr}$ values in the Valhalla complex have been explained by *Gordon et al.* [2009] as recording the signature of fluids from the deep crust driven by metamorphic devolatization and igneous crystallization. Cenozoic metaluminous plutons and supracrustal volcanic rocks in

Table 2. Parameters Used in AFC Modeling of the Different Crustal and Mantle Reservoirs in the Region of the ARG

Reservoirs	$^{87}Sr/^{86}Sr$	Sr ppm	Bulk *D* Sr	ε_{Nd}	Nd ppm	Bulk *D* Nd	ε_{Hf}	Hf ppm	Bulk *D* Hf	$\delta^{18}O_{wr}$	Δ
Stage I: Assimilation of Basalt and Mafic Lower Crust (r = 0.7)											
Average mantle (pristine magma I)	0.7069	335	0.10	−2.5	13.0	0.18	−2.5	3.4	0.20	5.6	0.1
Lower crust	0.7170	140	0.10	−25.0	33.0	0.18	−32.0	3.8	0.20	9.5	0.1
Stage IIa: Assimilation of Mixed Magma and Middle Crust (r = 0.56)											
Mixed magma (*F* = 0.76)	0.7088	440	2.2	−16.0	17.8	0.54	−14.6	4.0	0.65	7.4	0.1
Middle crust	0.7200	38	2.2	−35.0	15.0	0.54	−45.0	6.0	0.65	6.8	0.1

the region of the Valhalla complex were not studied. In contrast to the results from the Valhalla complex, most of our $\delta^{18}O_{zr}$ results indicate zircon crystallization from a magma that has a zircon oxygen isotopic composition similar to the mantle ($\delta^{18}O_{zr} = 5.3 \pm 0.6‰$ 2σ) [*Valley et al.*, 1998, 2005; *Valley*, 2003; *Grimes et al.*, 2011] and a crustal source represented by the inherited zircon cores in the Cenozoic magmas ($\delta^{18}O_{zr} = 5.6 \pm 0.2‰$; Figure 3) [*Strickland et al.*, 2011b; this study].

5.6. In Situ Zircon LA-ICP-MS Hf Isotope Analyses

[31] The initial Hf-isotope compositions of the Cenozoic zircon grains have $\varepsilon_{Hf(t)}$ values ranging from −15 to −42 (Figure 10b). These zircons define a trend of decreasing $\varepsilon_{Hf(t)}$ values through time (Figure 10b), with the oldest zircons (~38 Ma) of the Emigrant Pass plutonic complex having the most radiogenic values (−15 to −20) and the youngest (28–25 Ma) phases of the Cassia plutonic complex having the least radiogenic $\varepsilon_{Hf(t)}$ values (−35 to −42). We calculated the Hf isotopic compositions of Archean zircon cores at 40 Ma ($\varepsilon_{Hf(40)}$), rather than at their crystallization age, in order to compare with the Hf isotopic compositions of the Cenozoic zircon growth. These inherited Archean cores have $\varepsilon_{Hf(40)} \approx -60$ (Figure 10b) and stand in stark contrast to the Cenozoic rims (~20–45 ε_{Hf} units). This clearly indicates that the zircon rims represent new zircon growth and not simply reconstituted Archean zircon.

5.7. Geochemical Modeling and Evaluation of Crustal Assimilation

5.7.1. Potential Crustal Sources

[32] For the purpose of modeling the petrogenesis of the Cenozoic magmas studied here, we made a series of simplifying assumptions (outlined below) about the composition of two possible average crustal reservoirs (middle and lower crust). We do not consider Proterozoic metapelites and quartzites to have been a significant source for Eocene and Oligocene magmas, despite their favorable bulk compositions for dehydration melting. This is because these rocks are not partially melted at the exposed levels of the crust, and they were probably not present at greater depth (for instance, underthrust beneath the region) because their detrital zircon signatures are not evident in the Cenozoic magmas studied (see also discussion in *Strickland et al.* [2011b]). Furthermore, the $\delta^{18}O_{zr}$ of most of the Cenozoic zircon is inconsistent with a metapelitic melt source with $\delta^{18}O_{wr}$ of >8‰.

[33] Archean granite, monzogranite, and tonalite exposed in the Albion–Raft River–Grouse Creek (ARG) metamorphic core complex today [*Compton et al.*, 1977; *Compton*, 1972, 1975] also likely underlie part of the crustal section beneath the ARG. The felsic rocks have highly evolved Sr and Nd isotopic compositions [*Strickland et al.*, 2011b]. If these compositions (Figure 8) are representative of these felsic rocks at depth, then they cannot be the only crustal source for the Cenozoic magmas (see discussion in *Strickland*

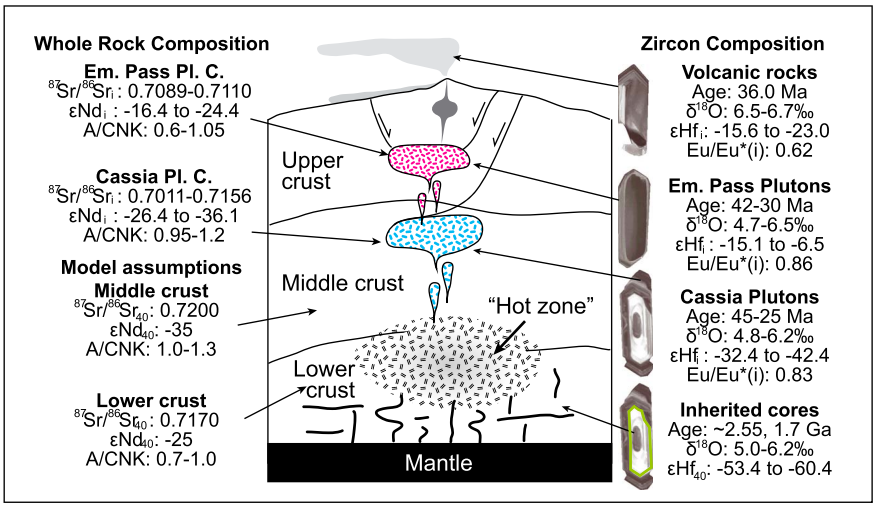

Figure 11. Schematic crustal column showing a summary of the zircon and whole-rock geochemical and geochronologic data from the igneous rocks of the ARG. Note that we present results from multiple crustal reservoirs and from igneous rocks at three crustal levels (middle crust, upper crust, and supracrustal volcanism). Also shown is the range of isotopic values for the middle and lower crust used in isotopic modeling.

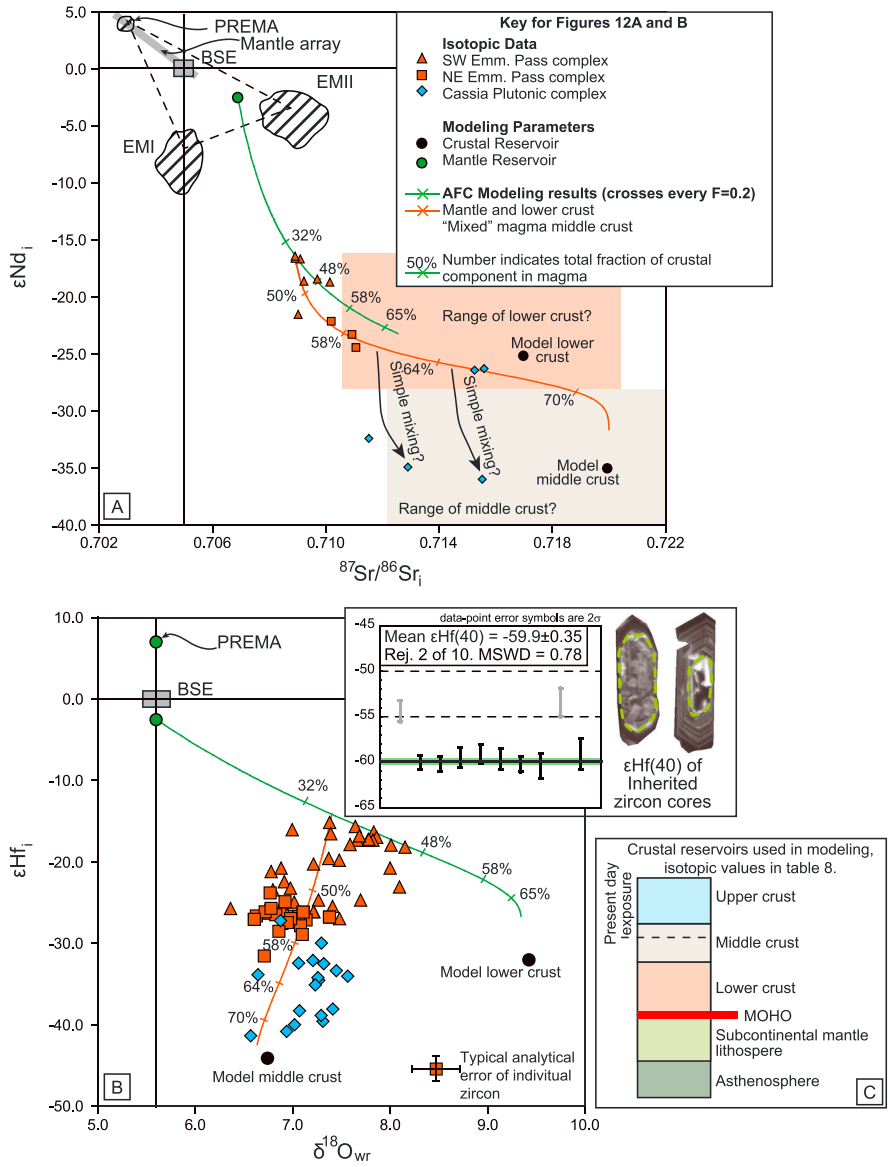

Figure 12. (a) Diagram showing the results from AFC $^{87}Sr/^{86}Sr_i$ versus $\varepsilon_{Nd(i)}$ isotopic modeling and the relative crust versus mantle components represented by the samples of this study (see the discussion in the text). (b) $\delta^{18}O_{wr}$ (calculated from zircon $\delta^{18}O$) versus $\varepsilon_{Hf(i)}$ compositions determined from individual zircon grains from samples of Cenozoic igneous rocks in the ARG metamorphic core complex. Also shown are the results from AFC isotopic modeling showing the relative crust versus mantle components represented by the samples in this study (see the discussion in the text). (c) Simplified pre-Cenozoic crustal column showing the approximate level of present-day exposure of deep rocks within the ARG.

et al. [2011b]). To model the isotopic composition of the potential middle crustal reservoir, we assumed that the most isotopically evolved samples of the Cenozoic plutons (Figure 8) represent nearly crustal melts with the approximate average composition of the middle crust. Thus, we estimate that the potential middle crust reservoir has a bulk isotopic composition of $^{87}Sr/^{86}Sr_{40} \approx 0.720$ and $\varepsilon_{Nd(40\ Ma)} \approx -35$ (Table 2), similar to values obtained from the most evolved Cenozoic plutonic rocks. The $\delta^{18}O_{wr}$ of this potential middle crust reservoir was estimated to be $\delta^{18}O_{wr} = 6.8‰$ based on isotopic values measured on Archean cores in Cenozoic zircons [*Strickland et al*., 2011b; this study] and a SiO_2 content of ~60–65%. The $\varepsilon_{Hf(40)}$ of the middle crustal reservoir was estimated as $\varepsilon_{Hf(40)} \approx -45$ [e.g., *Vervoort et al*., 2011] (Table 2 and Figures 11 and 12). This estimated whole-rock $\varepsilon_{Hf(40)}$ value for the middle crust is consistent with the composition of inherited zircon cores from the Cenozoic magmas ($\varepsilon_{Hf(40)} \approx -60$; Figure 12).

[34] Rocks from the deeper parts of the crust are not exposed in the ARG, but the potential lower crust reservoir would be made up of granulites, representing depths of >30km. The average Sr and Nd isotopic composition of the potential lower crust reservoir was estimated to have a similar isotopic composition to measured values from the amphibolite sample collected from the ARG (RR-5a; Figure 8). The lower crustal reservoir is estimated to have an average

$^{87}Sr/^{86}Sr_{40} = 0.717$ and $\varepsilon_{Nd(40\ Ma)} = -25$, (Table 2 and Figure 12). The $\delta^{18}O_{wr}$ of the potential lower crust reservoir was estimated from the range of $\delta^{18}O_{wr}$ of Cenozoic magmas (6.8–7.8‰) and the reasonable assumption that these Cenozoic magmas represent mixtures between the lower crust and the mantle ($\delta^{18}O_{wr} = 5.6$‰) [*Valley*, 2003] (Figure 10a). To generate the range of $\delta^{18}O_{wr}$ in Cenozoic magmas (6.8–7.8‰), the potential lower crustal reservoir must have a $\delta^{18}O_{wr}$ of about 9.5‰ [e.g., *Peck et al*., 2010]. The $\varepsilon_{Hf(40\ Ma)}$ of the lower crustal reservoir was estimated as $\varepsilon_{Hf(40\ Ma)} \approx -32$ (Table 2 and Figures 11 and 12).

5.7.2. Isotopic Modeling

[35] To model and evaluate the relative roles and components of mantle versus crustal material in Cenozoic magmas of the ARG, we used the equations of simultaneous assimilation and fractional crystallization (AFC) derived by *DePaolo* [1981] and the equation for estimating the ratio of mass of assimilated crust versus initial mass of magma by *Aitcheson and Forrest* [1994]. We have modeled the isotopic data (Sr, Nd, O, and Hf) together with the Sr, Nd, and Hf elemental compositions and tried a variety of reasonable values for the independent variables, including assimilation and fractional crystallization rates (*r* value in *DePaolo* [1981]) and bulk partition coefficients (all values used are reported in Table 2). We used a two-stage assimilation model for magma genesis [e.g., *Grunder*, 1993] that involves an initial high-temperature interaction of mantle-derived basalts with partial melts from a potential lower crust reservoir (Figures 11 and 12 and Table 2), with high assimilation and fractional crystallization rates, as shown in Figures 12a and 12b. This mixed magma assimilated variable amounts of partial melts from the potential middle crust reservoir in its second stage of assimilation (Figures 12a and 12b).

[36] The nature of potential asthenospheric or lithospheric mantle reservoirs contributing melts to the lower crust during the Cenozoic is not well constrained, primarily because of the extensive contamination of mantle-derived magmas by varying amounts of crustal melts. We estimated an isotopic composition of mantle-derived basalts based on the average composition of three mantle reservoirs (PREMA, EMI, and EMII; Figure 12) using the range of values summarized in *Rollinson* [1993]. The isotopic composition for the average mantle-derived basalt used for modeling is summarized in Table 2.

[37] The Sr-Nd-O-Hf isotopic compositions of magmas predicted from our AFC model [*DePaolo*, 1981] are compared to the measured whole-rock values ($^{87}Sr/^{86}Sr_i$-$\varepsilon_{Nd(i)}$; Figure 12a) and the measured isotopic values of individual Cenozoic zircon grains, corrected for whole-rock compositions ($\delta^{18}O_{wr}$-$\varepsilon_{Hf(i)}$; Figure 12b). This comparison (Figure 12) indicates that Cenozoic magmas analyzed in the ARG could have assimilated variable amounts of partial melts from the lower crust reservoir as well as partial melts from the potential middle crust reservoir (Figure 12). More specifically, our modeling indicates that the oldest (SW) phase of the EPC could represent the result of first-stage mixing of 60–50% mantle-derived melt with 40–50% partial melt of our assumed potential mafic crust reservoir (Figure 12). The composition and isotopic values of the younger NE phase of the EPC are best explained by a second-stage assimilation of magmas similar to those of the SW phase of the EPC, with partial melts of the potential middle crust reservoir, representing hybrids of 55–40% mantle-derived melts and 45–60% total crustal melt (from partial melts of two potential crustal reservoirs; Figure 12b). Finally, the isotopic compositions of the magmas from the CPC are best explained by assimilating hybrid magmas (similar to those of the SW phase of the EPC), with partial melts of potential lower and middle crust reservoirs (Figure 12). Some samples from the CPC could represent hybrid magmas composed of ~30% mantle-derived basalt and ~70% crustal melt, and some samples that have very negative $\varepsilon_{Nd(i)}$ may represent simple mixtures between hybrid Cenozoic magmas and Archean crustal melts (Figure 12).

8. Discussion

[38] The results of this study combined with data from *Egger et al*. [2003] and *Strickland et al*. [2011b] offer new constraints on the origin of Cenozoic magmatic rocks of the ARG metamorphic core complex. The geochronologic data indicate that the composite Emigrant Pass plutonic complex (EPC) and its local volcanic equivalents were the result of multiple periods of intrusion over a period of ~9 Ma, from ~41 to 32 Ma (Figure 5). The O and Hf isotopic results presented here illustrate that the Cassia plutonic complex (CPC, blue symbols in Figures 8, 9, 10, and 12) and the Emigrant Pass plutonic complex (EPC, red symbols in Figures 8, 9, 10, and 12) exhibit a continuous range of overlapping isotopic values (Figures 10 and 11). The 36.3 Ma volcanic sample (GC-1) hosts zircon has the highest measured $\delta^{18}O_{zr}$ values (6.5–6.8‰; Figures 10a and 11) and the least negative $\varepsilon_{Hf(i)}$ values (−16 to −23), but these values overlap the range of measured isotopic values (both Hf and O) of zircon from the Emigrant Pass plutonic complex (Figures 10b and 11). These data are compatible with the possibility that the vitric tuff represents the erupted volcanic equivalent of the granodioritic SW phase of the EPC.

[39] The good overlap in age and geochemical composition between the earliest phase of magmatism within the ARG and regional volcanism across northeastern Nevada (Figures 1, 5, 6, and 7) suggests that the Cenozoic magmas of the ARG are part of this regional magmatic event. Thus, it is reasonable to infer that Cenozoic magmatism in and around the ARG may be also the product of crustal melting by the addition of mafic magmas with a "subduction-like" mantle source (high fO_2 and high fH_2O) to the crust during the removal of the Farallon slab (Figures 13a and 13b), as initially suggested by *Armstrong and Ward* [1991], *Humphreys* [1995], and *Humphreys et al*. [2003].

[40] Our isotopic results indicate that decompression melting of metapelitic crust alone, as it has been proposed in other core complexes [e.g., *Teyssier and Whitney*, 2002; *Gordon et al*., 2008], is an unlikely mechanism of the formation of the Cenozoic magmas in the ARG. This process would produce only smaller, more strongly peraluminous plutons with no eruptive equivalents, highly variable evolved $^{87}Sr/^{86}Sr_i$ (given the variable Proterozoic ages of the sedimentary protoliths), and high (>8‰) $\delta^{18}O_{wr}$ values. None of these specific properties characterize the Cenozoic magmas of the ARG; however, some of the late and evolved phases of the CPC may represent magmas that are crustal melts. We acknowledge that melting and assimilation of the crust in the Cenozoic may have been enhanced not only by the input of basaltic magmas in the crust but also by the buildup

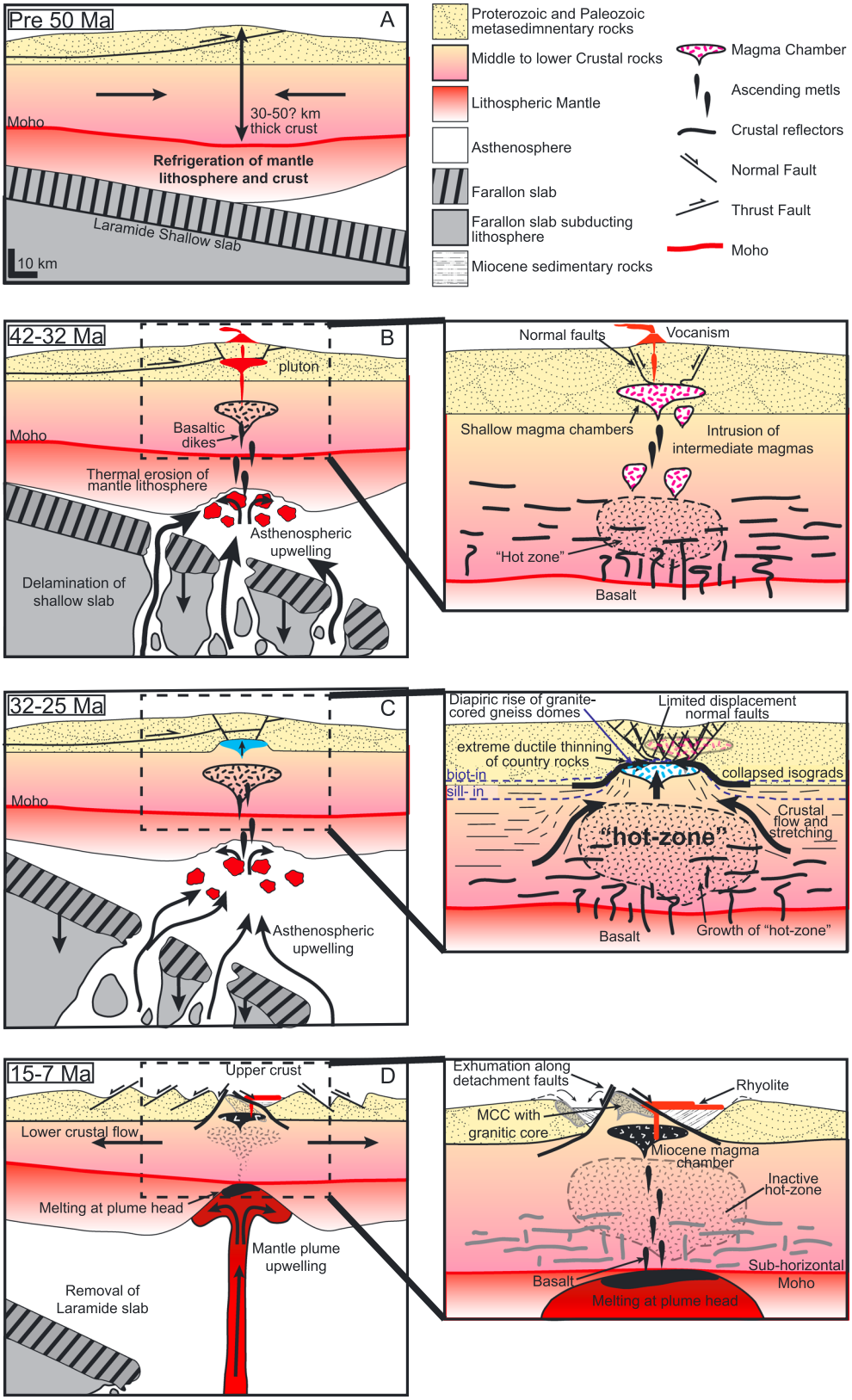

Figure 13. Cartoon summarizing the tectonic model proposed to explain the timing of the formation of the gneiss domes in the ARG and how it relates to regional tectonic events. For a detailed discussion, see text.

ofradiogenic heat and the perturbation of geothermal gradients following Mesozoic shortening (Figure 13a) [e.g., *Thompson*, 2000; *Miller and Gans*, 1989; *Clark et al*., 2011].

[41] The continuum of zircon ages ranging from ~41 to 25 Ma, between the EPC and the Cassia plutonic complex (CPC; Figure 5), their whole-rock geochemistry (Figures 6–8), and overlapping zircon trace element and isotopic compositions (Figures 9 and 10) indicate that these two plutonic suites shared a common deep magmatic source. This source was probably a broader, more regionally developed, "hot zone" [*Hildreth and Moorbath*, 1988] (Figures 11, 13b, and 13c) which evolved with time and was active for at least ~16 Myr (from 41 to 25 Ma), giving rise to magmas that crystallized as plutons in the middle (CPC) to upper crust (EPC). Based on modeling of the existing isotopic data (whole-rock Sr-Nd and zircon O and Hf isotopes) from the Cenozoic magmas of the ARG, this hot zone is most likely the result of the interaction of mantle-derived basalts with partial melts from heterogeneous Archean rocks at depth in the crust that have a less variable Sr-Nd composition than the exposed Archean crust in the region. This isotopic data preclude in situ partial melting of the Archean crust to form all the magmas in the ARG and require the rise of the magmas from the deeper crust to their current level of intrusion (Figures 11 and 13).

[42] The isotopic evolution of the Cenozoic magmas through time, coupled with our modeling of this evolution (Figures 10 and 12), suggests that this hot zone records increasing amounts of hybridization of mantle-derived basalts with crustal melts through time and that by Oligocene times, large-scale crustal melting gave rise to plutons that have large (~70%) crustal components, with some plutons constituting large degrees of crustal component (close to pure crustal melts; Figure 12). The high assimilation and fractional crystallization rates ($r = 0.56$–0.7; Table 2) used in our modeling to explain the observed isotopic compositions of the Cenozoic magmas indicate that the middle and lower crust remained at elevated temperatures (above the solidus of the crust) for a long period of time, at least for the time interval 41–25 Ma. This relatively long-lived magmatic system and the implied presence of molten crust beneath the ARG have profound effects on the strength and mobility of the deep crust during the Oligocene.

[43] Many studies have documented that partially molten crust is weaker and able to undergo crustal flow [e.g., *Teyssier and Whitney*, 2002; *Whitney et al*., 2004; *Kruckenberg et al*., 2008]. Here we infer that the prolonged flux of mafic magmas into the lower crust (Figure 13), documented by the geochemical and isotopic data described in this study, resulted in heating, melting, and weakening of the lower and middle crust. This facilitated the mobilization and rise of magmas with large crustal components from ~32 to 25 Ma which intruded during extension [*Strickland et al*., 2011a, 2011b; *Konstantinou et al*., 2012]. It is these younger magmas that are temporally and spatially associated with high-strain thinning of cover and wall rocks during the formation of the gneiss domes (see section 3.1 and Figure 13c) [e.g., *Armstrong*, 1963, 1968b; *Todd*, 1980; *Saltzer and Hodges*, 1998; *Sullivan*, 2008; *Strickland et al*., 2011a, 2011b; *Konstantinou et al*., 2012]. The formation of the synextensional gneiss domes was protracted and diachronous in the ARG with high-strain ductile fabrics and metamorphism developed adjacent to the individual granitic plutons and plutonic complexes whose emplacement spanned 32–25 Ma [e.g., *Egger et al*., 2003; *Strickland et al*., 2011a, 2011b; *Konstantinou et al*., 2012] (Figure 13c).

[44] We propose that mantle-driven magmatism in the ARG resulted in deep crustal melting, and the presence of partially molten crust and the magmas may provide density and viscosity anomalies that facilitated deep crustal flow and relative rise of flowing rocks in a way similar to the diapiric processes modeled by *Rey et al*. [2009a, 2009b, 2011] and *Tirel et al*. [2004]. The rise and crystallization of water-rich, peraluminous plutons to middle crustal depths (12–15 km) in the Oligocene were not accompanied by surface volcanism after ~32 Ma. The intrusive ages of these granites, in fact, correspond in time to the regional northern Basin and Range gap in volcanism (Figure 1b). By decreasing the energy lost from the middle crust through emplacement of shallow plutons and volcanic eruptions, the observed decrease in volcanism after ~32 Ma may have driven a positive feedback loop that enhanced crustal melting deeper in the crust.

9. Conclusions

[45] This study provides evidence to support the idea that the Cenozoic tectonic evolution of the ARG metamorphic core complex is the result of protracted (at least ~16 Ma) heating and partial melting of the deep crust, driven by the input of mantle-derived magmas. Based on the age and geochemistry of the oldest Cenozoic magmas studied, it is reasonable to conclude that the geodynamic processes driving the input of mantle-derived magmatism into the crust were the same as those responsible for generating the broader and more regional southward migration of volcanism charted across the western Cordillera (Figure 1). This magmatism has been attributed to the removal of the shallowly dipping Farallon slab, accompanied by asthenospheric upwelling and melting of lithospheric mantle, followed by heating and partial melting of the lower crust [e.g., *Armstrong and Ward*, 1991; *Humphreys*, 1995; *Humphreys et al*., 2003].

[46] Based on the similarity of their ages (Figure 5), whole-rock major and trace elements (Figures 6 and 7), whole-rock Sr-Nd isotopes (Figure 8) and zircon trace element (Figure 9), and zircon oxygen and Hf-isotope compositions (Figure 10), we have inferred that the 41–32 Ma Emigrant Pass plutonic complex and the 32–25 Ma Cassia plutonic complex (Figure 2) have a common origin and share a deep crustal "hot-zone" (Figures 11 and 13). This large middle crustal Eocene-Oligocene "hot-zone" played an important role in the thermomechanical evolution of the deeper crust beneath the ARG because it led to enhanced crustal flow at depth and the development and rise of synextensional granite-cored gneiss domes during extensional thinning and stretching of their roof and wall rocks. Specifically, our results suggest that mantle-derived magmatism plays a fundamental role in adding energy and mass to the lower crust, leading to deep crustal melting, weakening, and flow. The possibility of mantle-derived magmatic addition to the crust should be taken to consideration in numerical modeling of crustal flow in extensional tectonic settings, as well as in modeling the results of thermochronologic studies in metamorphic core complexes.

[47] **Acknowledgments.** We would like to thank the Stanford Graduate Fellowship, the ExxonMobil Science grant, the Leventis Foundation, and the Stanford McGee grant for providing financial support for this project. Support was also provided by the National Science Foundation Tectonics Division, grants EAR-0809226 and EAR-0948679, awarded to E. Miller. Gail Mahood, Marty Grove, and Simon Klemperer provided helpful discussions and insights that greatly improved this manuscript. This manuscript was improved by the comments of two anonymous reviewers. Noriko Kita and Kouki Kitajima are thanked for assistance with SIMS analysis of oxygen isotope ratios. WiscSIMS is partially supported by NSF-EAR grants 0319230, 0744079, and 1053466. The WSU Radiogenic Isotope and Geochronology Laboratory is partially supported by NSF-EAR grants 0844149, 1019877, and 1119237. Karrie Weaver and Caroline Harris are thanked for their help with the whole-rock Sr and Nd isotope analyses.

References

Aitcheson, S. J., and A. H. Forrest (1994), Quantification of crustal contamination in open magmatic systems, *J. Petrol.*, *35*(2), 461–488, doi:10.2113/gscanmin.45.1.43.

Akinin, V. V., E. L. Miller, and J. L. Wooden (2009), Petrology and geochronology of crustal xenoliths from the Bering Strait region: Linking deep and shallow processes in extending continental crust, in *Crustal Cross Sections from the Western North American Cordillera and Elsewhere: Implications for Tectonic and Petrologic Processes*, Spec. Pap. Geol. Soc. Am., vol. 456, R. B. Miller and A. W. Snoke, pp. 39–68, Geological Society of America, Boulder, CO, doi:10.1130/2009.2456(02).

Amato, J. M., and E. L. Miller (2004), Geologic map summary of the evolution of the Kigluaik mountains gneiss dome, Seward peninsula, Alaska, *Spec. Pap. Geol. Soc. Am.*, *380*, 295–306, doi:10.1130/0-8137-2380-9.295.

Amato, J. M., J. E. Wright, P. B. Gans, and E. L. Miller (1994), Magmatically induced metamorphism and deformation in the Kigluaik gneiss dome, Seward peninsula, Alaska, *Tectonics*, *13*(3), 515–527, doi:10.1029/93TC03320.

Amato, J. M., E. L. Miller, and K. A. Hannula (2002), Orthogonal flow directions in extending continental crust: An example from the Kigluaik gneiss dome, Seward peninsula, Alaska, *Spec. Pap. Geol. Soc. Am.*, *360*, 133–146, doi:10.1130/0-8137-2360-4.133.

Armstrong, R. L. (1963), Geochronology and geology of the eastern Great Basin in Nevada and Utah, PhD thesis, Yale Univ., New Haven, Conn.

Armstrong, R. L. (1968a), Pre-tertiary stratigraphy of the Albion range, southern Idaho, *Spec. Pap. Geol. Soc. Am.*, *101*, 384–385.

Armstrong, R. L. (1968b), Mantled gneiss domes in the Albion range, southern Idaho, *Geol. Soc. Am. Bull.*, *79*(10), 1295–1314, doi:10.1130/0016-7606(1968)79[1295:MGDITA].

Armstrong, R. L. (1982), Cordilleran metamorphic core complexes—From Arizona to southern Canada, *Annu. Rev. Earth Planet. Sci.*, *10*, 129–154, doi:10.1146/annurev.ea.10.050182.001021.

Armstrong, R. L., and F. A. Hills (1967), Rb-Sr and K-Ar geochronologic studies of mantled gneiss domes, Albion Range, southern Idaho, USA, *Earth Planet. Sci. Lett.*, *3*, 114–124, doi:10.1016/0012-821X(67)90021-0.

Armstrong, R. L., and P. L. Ward (1991), Evolving geographic patterns of Cenozoic magmatism in the North American Cordillera: The temporal and spatial association of magmatism and metamorphic core complexes; mid-tertiary Cordilleran magmatism; plate convergence versus intraplate processes, *J. Geophys. Res.*, *96*(B8), 13,201–13,224, doi:10.1029/91JB00412.

Axen, G. J., W. J. Taylor, and J. M. Bartley (1993), Space-time patterns and tectonic controls of tertiary extension and magmatism in the Great Basin of the western United States, *Geol. Soc. Am. Bull.*, *105*(1), 56–76, doi:10.1130/0016-7606(1993)105<0056:STPATC>2.3.CO;2.

Baker, W. H. (1959), Geologic setting and origin of the Grouse Creek pluton, Box Elder County, Utah, PhD thesis, Univ. of Utah, Salt Lake City.

Barth, A. P., and J. L. Wooden (2010), Coupled elemental and isotopic analyses of polygenetic zircons from granitic rocks by ion microprobe, with implications for melt evolution and the sources of granitic magmas, *Chem. Geol.*, *277*, 149–159, doi:10.1016/j.chemgeo.2010.07.017.

Bennett, E. H. (1986), Relationship of the trans-Challis fault system in central Idaho to Basin and Range extensions, *Geology 14*, 481–484, doi:10.1130/0091-7613(1986)14<481:ROTTFS>2.0.CO;2.

Best, M. G., and E. H. Christiansen (1991), Limited extension during peak tertiary volcanism, Great Basin of Nevada and Utah; mid-tertiary Cordilleran magmatism; plate convergence versus intraplate processes, *J. Geophys. Res.*, *96*(B8), 13,509–13,528.

Breitsprecher, K., D. J. Thorkelson, T. W. Groome, and J. Dostal (2003), Geochemical confirmation of the Kula-Farallon slab window beneath the pacific northwest in Eocene time, *Geology*, *31*(4), 351–354, doi:10.1130/0091-7613(2003)031<0351:GCOTKF>2.0.CO;2.

Brooks, W. E.,C. H. Thorman, and L. W. Snee (1995), The $^{40}Ar/^{39}Ar$ ages and tectonic setting of the middle Eocene northeast Nevada volcanic field, *J. Geophys. Res.*, *100*(B6), 10,403–10,416, doi:10.1029/94JB03389.

Burchfiel, B. C., D. S. Cowan, and G. A. Davis (1992), Tectonic overview of the Cordilleran orogen in the western United States, in *The Cordilleran Orogen: Conterminous U.S. Geology of North America*, vol. G-3, edited by B. C. Burchfiel, P. W. Lipman, and M. L. Zoback, 725 pp., Geol. Soc. of Am., Boulder, Colo.

Burton, B. R. (1997), Structural geology and emplacement history of the Harrison Pass pluton, central Ruby Mountains, Nevada, PhD thesis, Univ. of Wyoming, Laramie.

Catchings, R. D. (1992), A relation among geology, tectonics, and velocity structure, western to central Nevada Basin and Range, *Geol. Soc. Am. Bull.*, *104*(9), 1178–1192, doi:10.1130/0016-7606(1992)104<1178:ARAGTA>2.3.CO;2.

Catchings, R. D., and W. D. Mooney (1991), Basin and Range crustal and upper mantle structure, northwest to central Nevada, *J. Geophys. Res.*, *96*(B4), 6247–6267, doi:10.1029/91JB00194.

Christiansen, R. L., and P. W. Lipman (1972), Cenozoic volcanism and plate tectonic evolution of the western United States. II. Late Cenozoic, *Philos. Trans. R. Soc. London A*, *271*, 249–284, doi:10.1098/rsta.1972.0009.

Christiansen, E. H., and M. McCurry (2008), Contrasting origins of Cenozoic silicic volcanic rocks from the western Cordillera of the United States, *Bull. Volcanol.*, *70*(3), 251–267, doi:10.1007/s00445-007-0138-1.

Christiansen, R. L., and R. S. Yeats (1992), Post-Laramide geology of the U.S. Cordilleran region, in *The Cordilleran Orogen: Conterminous U.S. Geology of North America*, vol. G-3, edited by B. C. Burchfiel, P. W. Lipman, and M. L. Zoback, pp. 261–406, Geol. Soc. of Am., Boulder, Colo.

Clark, C., I. C. W. Fitzsimons, D. Healy, and S. L. Harley (2011), How does the continental crust get really hot?, *Elements*, *7*, 235–240.

Compton, R. R. (1972), Geologic map of the Yost quadrangle, Box Elder county, Utah, and Cassia county, Idaho, *Miscellaneous Geologic Investigations*, vol. map I-672, U.S. Geol. Surv., Washington, D. C.

Compton, R. R. (1975), Geologic map of the Park valley quadrangle, Box Elder county, Utah and Cassia county, Idaho, *Miscellaneous Investigations Series*, vol. map I-873, U.S. Geol. Surv., Reston, Va.

Compton, R. R. (1983), Displaced Miocene rocks on the west flank of the Raft River–Grouse Creek core complex, Utah: Tectonic and stratigraphic studies in the eastern Great Basin, *Mem. Geol. Soc. Am. Bull.*, *157*, 271–279.

Compton, R. R., V. R. Todd, R. E. Zartman, and C. W. Naeser (1977), Oligocene and Miocene metamorphism, folding, and low-angle faulting in northwestern Utah, *Geol. Soc. Am. Bull.*, *88*(9), 1237–1250, doi:10.1130/0016-7606(1977)88<1237:OAMMFA>2.0.CO;2.

Coney, P. J. (1980), Cordilleran metamorphic core complexes: An overview, *Mem. Geol. Soc. Am. Bull.*, *153*, 7–31.

Coney, P. J., and T. A. Harms (1984), Cordilleran metamorphic core complexes: Cenozoic extensional relics of Mesozoic compression, *Geology*, *12*(9), 550–554, doi:10.1130/0091-7613(1984)12<550:CMCCCE>2.0.CO;2.

DeCelles, P. G. (1994), Late Cretaceous–Paleocene synorogenic sedimentation and kinematic history of the Sevier thrust belt, northeast Utah and southwest Wyoming, *Bull. Geol. Soc. Am.*, *106*(1), 32–56, doi:10.1130/0016-7606(1994)106<0032:LCPSSA>2.3.CO;2.

DeCelles, P. G., and J. C. Coogan (2006), Regional structure and kinematic history of the Sevier fold-and-thrust belt, central Utah, *Geol. Soc. Am. Bull.*, *118*(7–8), 841–864, doi:10.1130/B25759.1.

DeCelles, P. G., T. F. Lawton, and G. Mitra (1995), Thrust timing, growth of structural culminations, and synorogenic sedimentation in the type Sevier orogenic belt, western United States, *Geology*, *23*(8), 699–702, doi:10.1130/0091-7613(1995)023<0699:TTGOSC>2.3.CO;2.

DePaolo, D. J. (1981), Trace element and isotopic effects of combined wallrock assimilation and fractional crystallization, *Earth Planet. Sci. Lett.*, *53*(2), 189–202, doi:10.1016/0012-821X(81)90153-9.

Dickinson, W. R. (2002), The Basin and Range Province as a composite extensional domain, *Int. Geol. Rev.*, *44*, 1–38, doi:10.2747/0020-6814.44.1.1.

Egger, A. E., T. A. Dumitru, E. L. Miller, C. F. I. Savage, and J. L. Wooden (2003), Timing and nature of Tertiary plutonism and extension in the Grouse Creek Mountains, Utah, *Int. Geol. Rev.*, *45*(6), 497–532, doi:10.2747/0020-6814.45.6.497.

Ferry, J. M., and E. B. Watson (2007), New thermodynamic models and revised calibrations for the Ti-in-zircon and Zr-in-rutile thermometers, *Contrib. Mineral. Petrol.*, *154*(4), 429–437, doi:10.1007/s00410-007-0201-0.

Fisher, C. M., D. Vervoort, and J. M. Hanchar (in review), Accurate Hf isotope determinations of complex zircons using the "laser ablation split stream" (LASS) method, *Geochem. Geophys. Geosyst.*

Gans, P. B., G. A. Mahood, and E. Schermer (1989), *Synextensional magmatism in the Basin and Range province: A case study from the eastern Great Basin*, Spec. Pap. Geol. Soc. Am., vol. 233, 53 p., Geol. Soc. of Am., Boulder, Colo.

Gashawbeza, E. M., S. L. Klemperer, C. K. Wilson, and E. L. Miller (2008), Nature of the crust beneath northwest Basin and Range province from teleseismic receiver function data, *J. Geophys. Res.*, *113*, B10308, doi:10.1029/2007JB005306.

Gordon, S. M., D. L. Whitney, C. Teyssier, M. Grove, and W. J. Dunlap (2008), Timescales of migmatization, melt crystallization, and cooling in a cordilleran gneiss dome: Valhalla complex, southeastern British Columbia, *Tectonics*, *27*, TC4010, doi:10.1029/2007TC002103.

Gordon, S. M., M. Grove, D. L. Whitney, A. K. Schmitt, and C. Teyssier (2009), Time-temperature-fluid evolution of migmatite dome crystallization: Coupled U/Pb age, Ti thermometry, and O isotopic ion microprobe depth profiling of zircon and monazite, *Chem. Geol.*, *262*(3–4), 186–201, doi:10.1016/j.chemgeo.2009.01.018.

Gottardi, R., C. Teyssier, A. Mulch, T. W. Vennemann, and M. L. Wells (2011), Preservation of an extreme transient geotherm in the Raft River detachment shear zone, *Geology*, *39*(8), 759–762.

Grimes, C. B., T. Ushikubo, B. E. John, and J. W. Valley (2011), Uniformly mantle-like $\delta^{18}O$ in zircons from oceanic plagiogranites and gabbros, *Contrib. Mineral. Petrol.*, *161*, 13–33, doi:10.1007/s00410-010-0519-x.

Grunder, A. L. (1993), Two-stage contamination during crustal assimilation: Isotopic evidence from volcanic rocks in eastern Nevada, *Contrib. Mineral. Petrol.*, *112*(2–3), 219–229.

Hauge, T. A., R. W. Allmendinger, C. Caruso, E. C. Hauser, S. L. Klemperer, S. Opdyke, and C. J. Potter (1987), Crustal structure of western Nevada from COCORP deep seismic-reflection data, *Bull. Geol. Soc. Am.*, *98*(3), 320–329, doi:10.1130/0016-7606(1987)98<320:CSOWNF>2.0.CO;2.

Hauser, E., C. Potter, T. A. Hauge, S. Burgess, S. Burtch, J. Mutschler, R. Allmendinger, L. Brown, S. Kaufman, and J. Oliver (1987), Crustal structure of eastern Nevada from COCORP deep seismic reflection data, *Bull. Geol. Soc. Am.*, *99*(6), 833–844, doi:10.1130/0016-7606(1987)99<833:CSOENF>2.0.CO;2.

Henry, C. D., J. P. Colgan, A. J. McGrew, A. W. Snoke, and M. E. Brueseke (2011), Timing, distribution, amount, style, and causes of Cenozoic extension, northern Great Basin, in *Geologic Field Trips to the Basin and Range, Rocky Mountains, Snake River Plain and Terranes of the U.S. Cordillera*, Geol. Soc. Am. Field Guide, vol. 21, edited by J. Lee and J. P. Evans, pp. 27–66, Geological Society of America, Boulder, CO.

Hildreth, W., and S. Moorbath (1988), Crustal contributions to arc magmatism in the Andes of central Chile, *Contrib. Mineral. Petrol.*, *98*(4), 455–489, doi:10.1007/BF00372365.

Holbrook, W. S., R. D. Catchings, C. M. Jarchow (1991), Origin of deep crustal reflections: Implications of coincident seismic refraction and reflection data in Nevada, *Geology*, *19*(2), 175–179, doi:10.1130/0091-7613(1991)019<0175:OODCRI>2.3.CO;2.

Humphreys, E. D. (1995), Post-Laramide removal of the Farallon slab, western United States, *Geology*, *23*(11), 987–990, doi:10.1130/0091-7613(1995)023<0987:PLROTF>2.3.CO;2.

Humphreys, E., E. Hessler, K. Dueker, G. L. Farmer, E. Erslev, and T. Atwater (2003), How Laramide-age hydration of North American lithosphere by the Faralon slab controlled subsequent activity in the western United States, *Int. Geol. Rev.*, *45*(7), 575–595, doi:10.2747/0020-6814.45.7.575.

Ickert, R. B., D. J. Thorkelson, D. D. Marshall, and T. D. Ullrich (2009), Eocene Adakitic volcanism in southern British Columbia: Remelting of arc basalt above a slab window, *Tectonophysics*, *464*(1–4), 164–185, doi:10.1016/j.tecto.2007.10.007.

Khattab, M. M. (1969), Gravity and magnetic surveys of the grouse creek mountains and the Raft River Mountains area and vicinity, Utah and Idaho, PhD thesis, Univ. of Utah, Salt Lake City.

Kiilsgaard, T. H., F. S. Fisher, and E. H. Bennett (1986), The trans-Challis fault system and associated precious metal deposits, Idaho, *Econ. Geol. Bull. Soc. Econ. Geol.*, *81*(3), 721–724, doi:10.2113/gsecongeo.81.3.721.

Kita, N. T., T. Ushikubo, and J. W. Valley (2009), High precision SIMS O-isotope analysis and the effect of sample topography, *Chem. Geol.*, *264*(1–4), 43–57.

Klemperer, S. L., T. A. Hauge, E. C. Hauser, J. E. Oliver, and C. J. Potter (1986), The MOHO in the northern Basin and Range province, Nevada, along the COCORP 40 degrees N seismic-reflection transect, *Bull. Geol. Soc. Am.*, *97*(5), 603–618, doi:10.1130/0016-7606(1986)97<603:TMITNB>2.0.CO;2.

Klemperer, S. L., E. L. Miller, A. Grantz, D. W. Scholl, and Bering-Chukchi Working Group (2002), Crustal structure of the Bering and Chukchi shelves: Deep seismic reflection profiles across the North American continent between Alaska and Russia, in *Tectonic Evolution of the Bering Shelf–Chukchi Sea–Arctic Margin and Adjacent Landmasses*, Spec. Pap. Geol. Soc. Am., vol. 360, edited by E. L. Miller, A. Grantz, and S. L. Klemperer, pp. 1–24, Geol. Soc. of Am., Boulder, Colo.

Konstantinou, A. (2011), Off-axis Snake River Plain magmatism along an active extensional detachment: An example from the Jim Sage volcanic suite, southern ID, *Abstracts With Programs*: *2011 GSA Annual Meeting*, 43(5), Abstract 191614.

Konstantinou, A., A. Strickland, E. L. Miller, and J. W. Wooden (2012), Multi-stage Cenozoic extension of the Albion–Raft River–Grouse Creek metamorphic core complex: Geochronologic and stratigraphic constraints, *Geosphere*, *8*(6), 1–38, doi:10.1130/GES00778.1.

Kruckenberg, S. C., D. L. Whitney, C. Teyssier, C. M. Fanning, and J. W. Dunlap (2008), Paleocene-Eocene migmatite crystallization, extension, and exhumation in the hinterland of the northern Cordillera: Okanogan dome, Washington, USA, *Bull. Geol. Soc. Am.*, *120*(7), 912, doi:10.1130/B26153.1.

Kruckenberg, S. C., O. Vanderhaeghe, E. C. Ferré, C. Teyssier, and D. L. Wjitney (2011), Flow of partially molten crust and the internal dynamics of a migmatite dome, Naxos, Greece, *Tectonics*, *30*, TC3001, doi:10.1029/2010TC002751.

Lackey, J. S., J. W. Valley, J. H. Chen, and D. F. Stockli (2008), Dynamic magma systems, crustal recycling, and alteration in the central Sierra Nevada batholith: The oxygen isotope record, *J. Petrol.*, *49*, 1397–1426, doi:10.1093/petrology/egn030.

Langenheim, V. E., D. M. Miller, T. J. Felger, M. L. Wells, G. C. Willis, and D. L. Clark (2011), New aeromagnetic survey reveals widespread quaternary and Neogene volcanic rocks and footwall structure in northwest Utah, *Abstracts With Programs*: *2011 Rocky Mountain/Cordilleran Joint GSA Meeting* (May 2011), 43(4), 49.

Lee, C. T. A. (2005), Trace element evidence for hydrous metasomatism at the base of the North American lithosphere and possible association with Laramide low-angle subduction, *J. Geol.*, *113*(6), 673–685, doi:10.1086/449327.

Lee, C. T. A. (2006), Chemical modification of lithosphere and the origin of intracontinental magmatism and deformation, *Geochim. Cosmochim. Acta*, *70*(18), A346–A346, doi:10.1016/j.gca.2006.06.701.

Martinez, C. M. (2000), Character of Miocene syn-tectonic sediments deposited adjacent to the Grouse Creek Mountains, northwestern Utah, 2000 Geological Society of America Annual Meeting, Abstracts With Programs, Geol. Soc. Am., 32(7), 44.

McFadden, R. R., C. S. Siddoway, C. Teyssier, and C. M. Fanning (2010), Cretaceous oblique extensional deformation and magma accumulation in the Fosdick Mountains migmatite-cored gneiss dome, West Antarctica, *Tectonics*, *29*, TC4022, doi:10.1029/2009TC002492.

Miller, D. M. (1978), Deformation associated with Big Bertha dome, Albion Mountains, Idaho, PhD thesis., Univ. of Calif., Los Angeles.

Miller, D. M. (1980), Structural geology of the northern Albion Mountains, south-central Idaho, *Mem. Geol. Soc. Am.*, *153*, 399–423.

Miller, D. M. (1983), Strain on a gneiss dome in the Albion mountains metamorphic core complex, Idaho, *Am. J. Sci.*, *283*(6), 605–632.

Miller, E., and P. B. Gans (1989), Cretaceous crustal structure and metamorphism in the hinterland of the Sevier thrust belt, western U.S. Cordillera, *Geology*, *17*(1), 59–62, doi:10.1130/0091-7613(1989)017<0059:CCSAMI>2.3.CO;2.

Miller, E. L., A. T. Calvert, and T. A. Little (1992), Strain-collapsed metamorphic isograds in a sillimanite gneiss dome, Seward Peninsula, Alaska, *Geology*, *20*(6), 487–490.

Miller, D. M., R. L. Armstrong, D. R. Bedford, and M. Davis (2008), Geologic map and digital data base of the Almo quadrangle and city of rocks national reserve, Cassia county, Idaho, *U.S. Geol. Surv. Open File Rep*., OF 2008-1103 (1 sheet, 2008): 36.

Miller, E. L., A. Konstantinou and A. Strickland (2012), Comment on "Geodynamics of synconvergent extension and tectonic mode switching: Constraints from the Sevier-Laramide orogen" by Michael L. Wells et al, *Tectonics*, *31*, TC4015, doi:10.1029/2012TC003103.

North American Volcanic and Intrusive Rock Database (NAVDAT) (2011), The Western North American Volcanic and Intrusive Rock Database, http://www.navdat.org/, accessed 3 October 2011.

Peck, W. H., C. C. Clechenko, M. A. Hamilton, and J. W. Valley (2010), Oxygen isotopes in the Grenville and Nain AMCG suites: Regional aspects of the crustal component in Massif anorthosites, *Can. Mineral.*, *48*, 763–786, doi:10.3749/canmin.48.4.763.

Rey, P. F., C. Teyssier, D. L. Whitney (2009a), Extension rates, crustal melting, and core complex dynamics, *Geology*, *37*(5), 391–394, doi:10.1130/G25460A.1.

Rey, P. F., C. Teyssier, and D. L. Whitney (2009b), The role of partial melting and extensional strain rates in the development of metamorphic core complexes, *Tectonophysics*, *477*(3–4), 135–144, doi:10.1016/j.tecto.2009.03.010.

Rey, P. F., C. Teyssier, S. C. Kruckenberg, and D. L. Whitney (2011), Viscous collision in channel explains double domes in metamorphic core complexes, *Geology*, *39*(4), 387, doi:10.1130/G31587.1.

Rollinson, H. R. (1993), *Using Geochemical Data: Evaluation, Presentation, Interpretation*, Longman Geochem. Ser., Longman, Harlow, Essex, U. K.

Saltzer, S. D., and K. V. Hodges (1998), The Middle Mountain shear zone, southern Idaho: Kinematic analysis of an early Tertiary high-temperature detachment, *Geol. Soc. Am. Bull.*, *100*, 96–103.

Stewart, J. H. (1980), Regional tilt patterns of late Cenozoic Basin-Range fault blocks, western United States, *Geol. Soc. Am. Bull., Part 1*, *91*(8), 460–464, doi:10.1130/0016-7606(1977)88<67:EPOCIR>2.0.CO;2.

Stewart, J. H., W. J. Moore, and I. Zietz (1977), East-west patterns of Cenozoic igneous rocks, aeromagnetic anomalies, and mineral deposits, Nevada and Utah, *Geol. Soc. Am. Bull.*, *88*, 67–77.

Strickland, A., E. L. Miller, and J. L. Wooden (2011a), The timing of Tertiary metamorphism and deformation in the Albion–Raft River–Grouse Creek metamorphic core complex, Utah and Idaho, *J. Geol.*, *119*(2), 185–206, doi:10.1086/658294.

Strickland, A., E. L. Miller, J. L. Wooden, R. Kozdon, and J. W. Valley (2011b), Syn-extensional plutonism and peak metamorphism in the Albion–Raft River–Grouse Creek metamorphic core complex, *Am. J. Sci.*, *311*(4), 261, doi:10.2475/04.2011.01.

Sullivan, W. A. (2008), Significance of transport-parallel strain variations in part of the Raft River shear zone, Raft River Mountains, Utah, USA, *J. Struct. Geol.*, *30*, 138–158, doi:10.1016/j.jsg.2007.11.007.

Teyssier, C., and D. L. Whitney (2002), Gneiss domes and orogeny, *Geology*, *30*(12), 1139–1142, doi:10.1130/0091-7613(2002)030<1139:GDAO>2.0.CO;2.

Thompson, A. B. (2000), Some space–time relationships for crustal melting and granitic intrusion at various depths, in *Understanding Granites: Integrating New and Classical Techniques*, Spec. Publ. Geol. Soc. London, vol. 168, edited by A. Castro, C. Fernandez, and J. L. Vigneresse, pp. 7–25, Geological Society of America, Boulder, CO.

Tirel, C., J.-P. Brun, and E. Burov (2004), Thermo-mechanical modeling of extensional gneiss domes, in *Gneiss Domes in Orogeny*, Spec. Pap. Geol. Soc. Am., vol. 380, edited by D. L. Whitney, C. Teyssier, and C. S. Siddoway, pp. 67–78, Geological Society of America, Boulder, CO.

Tirel, C., J.-P. Brun, and E. Burov (2008), Dynamics and structural development of metamorphic core complexes, *J. Geophys. Res.*, *113*, B04403, doi:10.1029/2005JB003694.

Todd, V. R. (1980), Structure and petrology of a Tertiary gneiss complex in northwestern Utah, *Mem. Geol. Soc. Am.*, *153*, 349–383.

Valley, J. W. (2003), O-isotopes in zircon, *Rev. Mineral. Geochem.*, *53*, 343–385.

Valley, J. W., and N. T. Kita (2009), In situ O-isotope geochemistry by ion microprobe, in *MAC Short Course: Secondary Ion Mass Spectrometry in the Earth Sciences*, vol. 41, edited by M. Fayek, pp. 19–63, Mineralogical Association of Canada, Toronto, Canada.

Valley, J. W., P. D. Kinny, D. J. Schulze, and M. J. Spicuzza (1998), Zircon megacrysts from kimberlite: O-isotope variability among mantle melts, *Contrib. Mineral. Petrol.*, *133*(1–2), 1–11, doi:10.1007/s004100050432.

Valley, J. W., J. S. Lackey, A. J. Cavosie, C. C. Clechenko, M. J. Spicuzza, M. A. Basei, and I. N. Bindeman (2005), 4.4 billion years of crustal maturation: O-isotope ratios of magmatic zircon, *Contrib. Mineral. Petrol.*, *150*(6), 561–580, doi:10.1007/s00410-005-0025-8.

Vanderhaeghe, O.,C. Teyssier, and R. Wysoczanski (1999), Structural and geochronological constraints on the role of partial melting during the formation of the Shuswap metamorphic core complex at the latitude of the Thor-Odin dome, British Columbia, *Can. J. Earth Sci.*, *36*(6), 917–943, doi:10.1139/e99-023.

Vervoort J. D., T. Plank, and J. Prytulak (2011), The Hf-Nd isotopic composition of marine sediments, *Geochim. Cosmochim. Acta*, *75*, 5903–5926, doi:10.1016/j.gca.2011.07.046.

Wells, M. L. (2009), Geologic map of the Kelton Pass quadrangle, Box Elder County, Utah, and Cassia County, Idaho, Miscellaneous Publication 09-3, Utah Geol. Surv., ISBN 1-55791-807-4.

Wells, M. L., L. W. Snee, and A. E. Blythe (2000), Dating of major normal fault systems using thermochronology: An example from the Raft River detachment, Basin and Range, western United States, *J. Geophys. Res.*, *105*(B7), 16,303–16,327, doi:10.1029/2000JB900094.

Wells, M. L., T. D. Hoisch, A. M. Cruz-Uribe, and J. D. Vervoort (2012), Geodynamics of synconvergent extension and tectonic mode switching: Constraints from the Sevier-Laramide orogen, *Tectonics*, *31*, TC1002, doi:10.1029/2011TC002913.

Wernicke, B. P. (1981), Low-angle normal faults in the Basin and Range Province: Nappe tectonics in an extending orogen, *Nature*, *291*(5817), 645–648, doi:10.1038/291645a0.

Wernicke, B. (1992), Cenozoic extensional tectonics of the U. S. Cordillera, in *The Cordilleran Orogen: Conterminous U.S*, Geol. North Am., vol. G-3, edited by B. C. Burchfiel, P. W. Lipman, and M. L. Zoback, pp. 553–581, Geol. Soc. of Am., Boulder, Colo.

Whitney D. L., C. Teyssier, and O. Vanderhaeghe (2004), Gneiss domes and crustal flow, *Spec. Pap. Geol. Soc. Am.*, *380*, 15–33.

Wright, J. E., and J. L. Wooden (1991), New Sr, Nd, and Pb isotopic data from plutons in the northern Great Basin; implications for crustal structure and granite petrogenesis in the hinterland of the Sevier thrust belt, *Geology*, *19*(5), 457–460, doi:10.1130/0091-7613(1991)019<0457:NSNAPI>2.3.CO;2.